2| Synthesis

2.1 INTRODUCTION

Polychlorotriphenylmethyl radicals are highly persistent due to the huge steric hindrance around the open-shell centre promoted by the *ortho* chlorine atoms of the triarylmethyl structure.[1] The same factor that confers such a high chemical and thermal stability, results crucial to explain the strong reaction conditions that have to be used for their preparation which consist in three different steps: I) Friedel-Crafts, II) deprotonation and III) oxidation reaction. As an example, here we show the synthesis of the trichlorotriphenylmethyl radical **12** (Scheme1). [2]

Step I) synthesis of the trichlorotriphenylmethane **11**, precursor of the radical **12**, consist in a triple Friedel-Crafts reaction which is not possible to take place in solution but in a high pressure reactor, at 80ºC, with an excess of trichlorobenzene and using $AlCl_3$ as a catalyst.

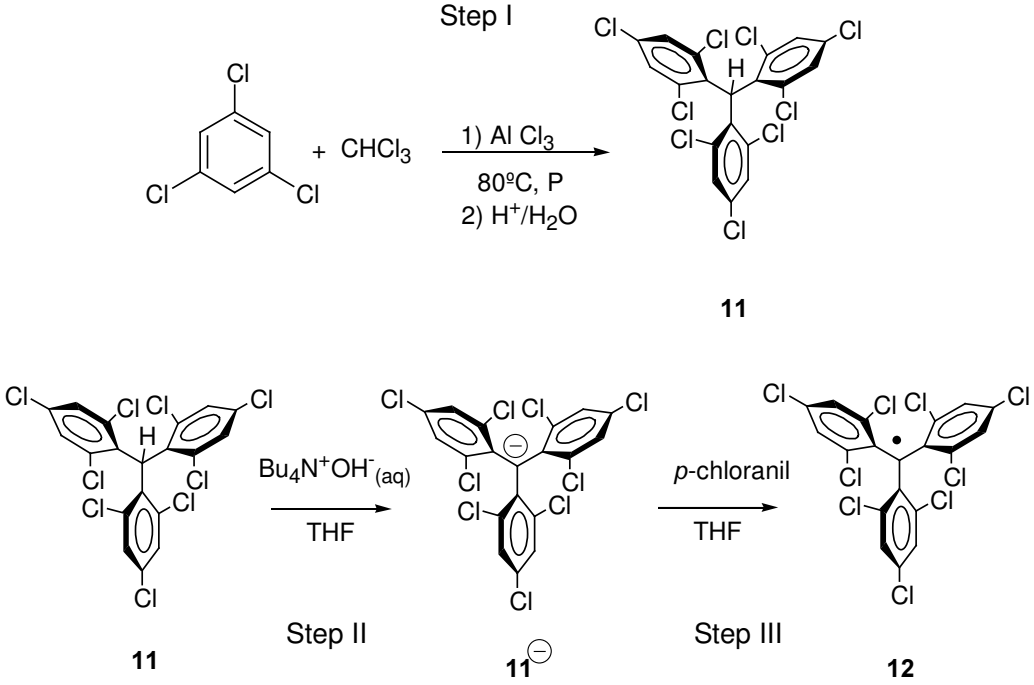

Scheme 1

Step II) synthesis of the trichlorotriphenylmethyl anion by adding an aqueous solution of tetra-(*n*-butyl)ammonium hydroxide to compound **11**. The small acidity of the central methylenic proton, in addition to its high steric hindrance, make the kinetic of the acid-base reaction very slow.

Step III) oxidation of the anionic species to radical **12**.[3] This step results straight being the largest inconvenient the manipulation of the radical species in solution, which has to be handle under red light to avoid any decomposition side-reaction.[4]
Step II) and III) in some cases take place in a one pot reaction depending on the oxidation potential of the reactants and the oxidizing agent used for the oxidation of the anion in step III.

Synthetic difficulties does not only arise during the synthesis of polychlorotriphenylmethyl radicals but also along their coupling reactions with ferrocene or ruthenocene aldehyde products due to the deactivation endorsed by the electron-withdrawing chlorine atoms in front of nucleophilic reactions. Two different coupling reactions have been performed A) condensation reaction of a functionalised polychlorotriphenylmethylradical to generate directly the radical species B) condensation reaction of a functionalised precursor of the trichlorotriphenylmethyl radical and subsequent generation of the radical species.

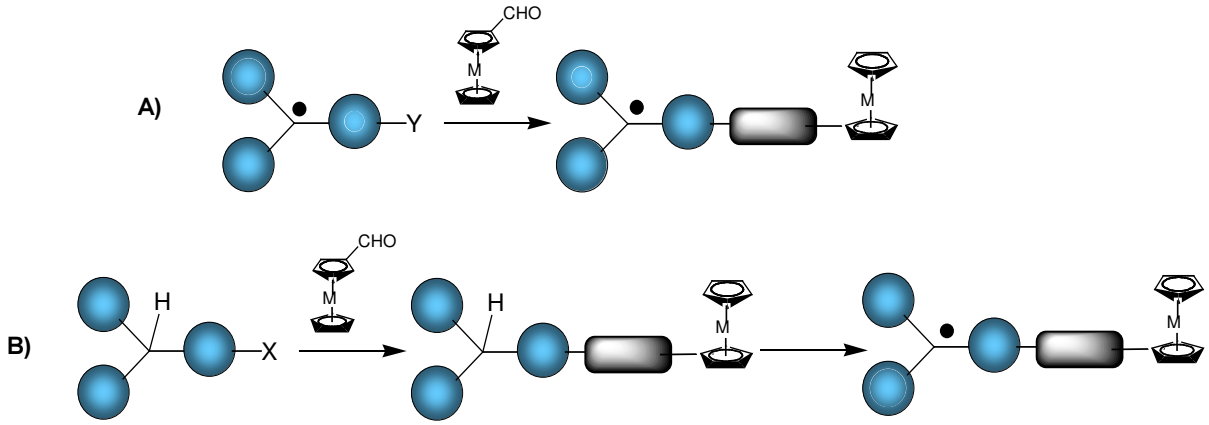

Scheme 2

Finally, it has to be emphasized that all compounds so far synthesized hereby reported have been fully characterized by different techniques such as elemental analysis, matrix assisted laser desorption time-of-flight (MALDI-TOF) mass spectrometry, HPLC, cyclic voltammetry, FT-IR, NMR, UV/Vis/ NIR, and EPR spectroscopy (see Experimental Part, Chapter 5).

2.2 SYNTHESIS OF FERROCECE-BASED 1-6

2.2.1 Synthesis of Ferrocenyl Schiff Based Polychlorotriphenylmethyl Radicals 3- 6

The synthesis of ferrocenyl Schiff base polychlorotriphenylmethyl radicals **3-6** is performed following the strategy A (see Scheme 2) for the coupling and involves two main steps. The first step is the generation of the (4-amino-2,6-dichlorophenyl)bis(2,4,6-trichlorophenyl)methyl radical (**15**) and the second step is the condensation reaction between the amino radical (**15**) and ferrocene monocarboxaldehyde for the synthesis of radicals **3** and **5** or nonamethyl ferrocene monocarboxadehyde for the synthesis of radicals **4** and **6**.

Step I) Synthesis of (4-amino-2,6-dichlorophenyl)bis(2,4,6-trichlorophenyl)methyl radical (15)

Radical **15** was obtained following the synthetic methodology previously described in the literature.[5] Initially, oxidation of radical **12**, which was obtained as previously described, with antimony pentachloride as the oxidation agent, yields the corresponding cationic derivative **13**. Then, ammonia gas was bubbled over a solution of **13** in methylenchloride followed by a reduction with $SnCl_2$ to obtain **15** as a dark-red microcrystalline solid with a 58% yield (Scheme 3).

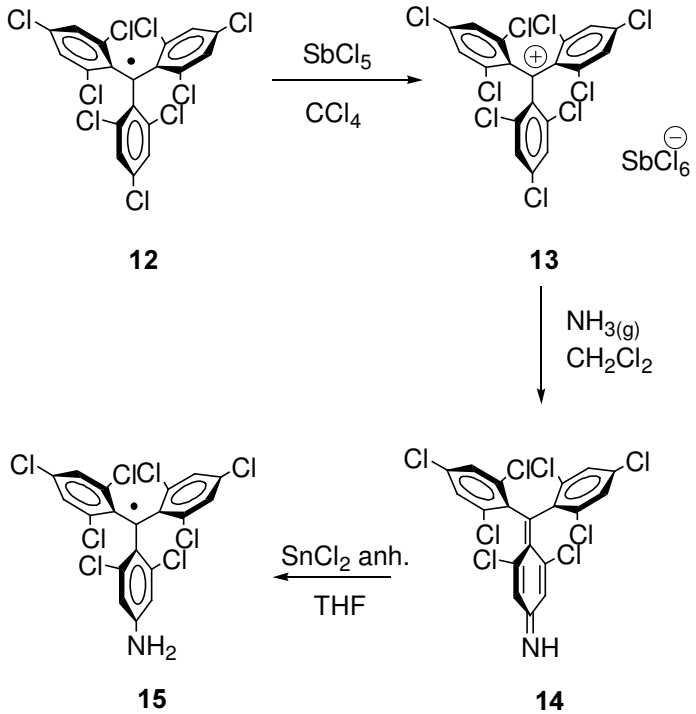

12 **13** **15** **14**

Scheme 3

*Step II) Condensation Reaction: Synthesis of (trans)-4-ferrocenylimine-2,6-dichlorophenyl -bis(2,4,6-trichlorophenyl) methyl radical (**3**) and (cis)-4-ferrocenylimine-2,6-dichlorophenyl-bis(2,4,6,trichlorophenyl) methyl (**5**)*

The condensation reaction between radical **15** and ferrocene monocarboxylaldehyde was carried out in a toluene solution using molecular sieves, as dehydrating agent. In that way the yield was improve by removing water molecules from the solution generated as side-product from the condensation reaction. The reaction is not stereoselective, reason why both isomers *trans* (radical **3**) and *cis* (radical **5**) were obtained and isolated as microcrystalline material from the mixture reaction as stable species in front of light and atmospheric oxygen. Isomer *trans* (radical **3**) can be isolated by recrystallization of the reaction mixture from a hexane solution with a 20% yield while isomer *cis* (radical **5**) was isolated by a chromatographic method using magnesium silicate (Florisil) as a chromatographic support and carbon tetrachloride as eluent with a 6% yield. The use of Florisil in the isolation of radical **3** is highly required since the presence of an *imine* group, which is very sensitive to the acidic points of the silica, makes problematic the use of silica gel as a chromatographic support for its purification. Single crystals of **3** for the X-ray structure analysis were grown by slow evaporation from a carbon tetrachloride/ hexanes (1/1) mixture (see Crystallographic Data, Chapter 6).

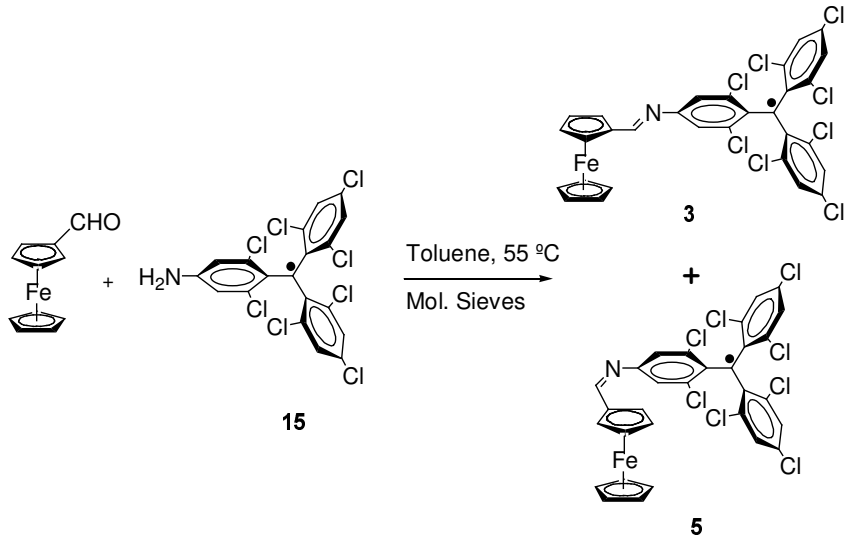

Scheme 4

*Step II) Condensation Reaction: Synthesis of (trans)-4-nonamethylferrocenyl imine-2,6-dichlorophenyl-bis(2,4,6-trichlorophenyl) methyl radical (**4**)*

The synthetic route and experimental conditions used for the obtaining of radical **4** are very similar to those previously described for the synthesis of radicals **3** and **5**. Radical **4** was synthesized by a condensation reaction between nonamethylferrocene monocarboxadehyde and radical **15**, as shown in Scheme 4. Even though the condensation reaction takes place following a similar mechanistic pathway than that previously described for the synthesis of radicals **3** and **5**, in the present case, the reaction rates are considerably slower probably due to a higher deactivation of the permethylated ferrocene aldehyde in front of a nucleophilic attack. Moreover, it has to be emphasized that only the *trans* isomer (radical **4**) was obtained and isolated as a stable species. The lack of the corresponding *cis* isomer (radical **6**) has been tentatively attributed to the presence of high steric interactions between methyl groups of the ferrocene unit and chlorine atoms of the tripheylmethyl radical. Finally, isomer *trans* (radical **4**) was purified by column chromatography using basic alumina as a chromatographic support and a mixture of hexane/carbon tetrachloride as eluent and a 20% yield for this reaction was obtained. This radical show a high persistency in solid or solution and also in front of oxygen or light.

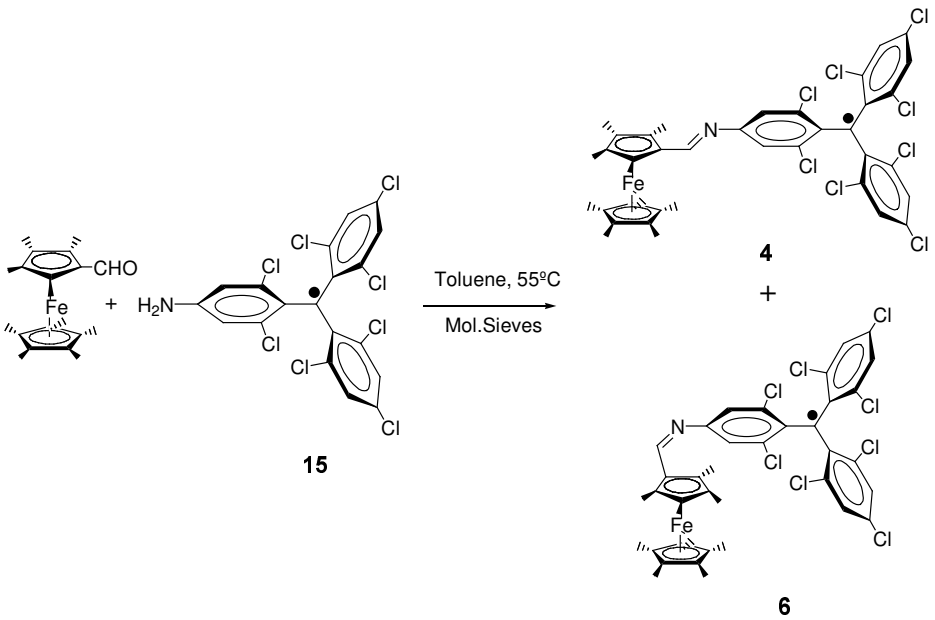

Scheme 5

2.2.2 Synthesis of (*trans*)-4-ferrocenylvinylene-2,3,5,6-tetrachlorophenyl-bis(pentachlorophenyl) methyl Radical 1

The synthetic route to prepare radical **1** is based on the strategy B) (see Scheme 2) for the coupling and involves three main steps: I) synthesis of the substituted phosphonium bromide **17**, II) Wittig reaction between the corresponding ferrocene carboxaldehyde derivative and the phosphonium bromide precursor **17** and III) sequent deprotonation and oxidation to yield the desired radical.

*I) Synthesis of the substituted phosphonium bromide **17***

As outlined in Scheme 6, treatment of the bromomethane derivative **16**,[6] with triphenylphosphine yielded the substituted phosphonium bromide **17**.[7]

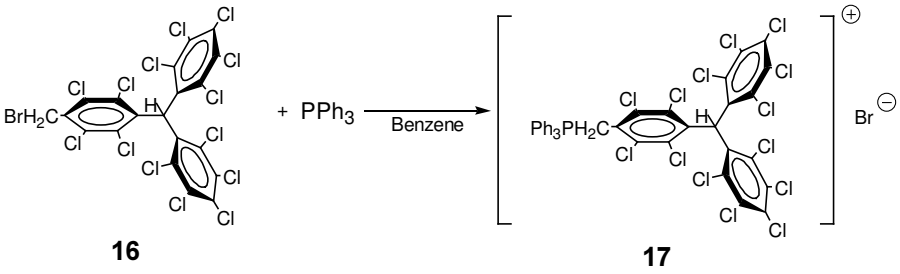

16 **17**

Scheme 6

II) Wittig reaction

The phosphonium bromide **17** is suspended in dry THF and treated with an equimolar amount of potassium *tert*-butoxide to yield the corresponding ylide. Then the ferrocene monocarboxaldehyde is added to give the desired (*trans*)-4-ferrocenylvinylene-2,3,5,6-tetrachlorophenyl-bis(pentachlorophenyl) methane (**18**) with a 53% yield. It was purified through a silica gel chromatographic column using hexane/ether 50% as eluent. Single crystals of **18** for the X-ray structure analysis were grown by slow evaporation from a methylene chloride (see Crystallographic Data, Chapter 6).

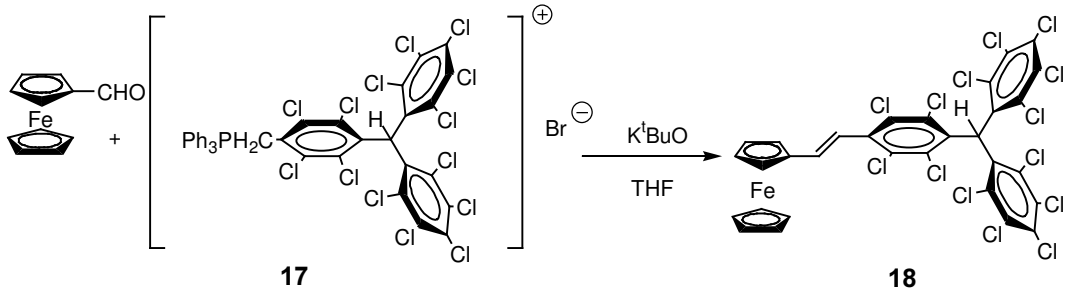

17 **18**

Scheme 7

The Wittig reaction between the phosphonium bromide precursor **17** and the ferrocene monocarboxaldehyde derivative is highly stereoselective, yielding exclusively the *trans* isomer **18** as ascertained by the characteristic coupling constant in the NMR spectrum (J=16.23Hz).[8] Such stereoselectivity is justified if we consider that the ylide derived from the phosphonium bromide is stabilized by the presence of the polychlorinated aromatic ring. Actually, the natural preference of ylides with electron withdrawing groups that stabilize the betaine form has been experimentally shown to give mainly the *trans* isomer.[9] In addition, the *cis/trans* isomer distribution of the Wittig products is also strongly influenced by the nature of the base used in the preparation of the ylide; being the potassium *tert*-butoxide, used in this work, the base of choice for maximizing the yields of *trans* olefins.[10,11]

III) Deprotonation and oxidation

The third step for the synthesis of radical **1** consists in a deprotonation of the triphenylmethane **18** and a subsequent oxidation of the resulting anion. An excess of an aqueous solution of tetra(*n*-butyl)ammonium hydroxide is added to a THF solution of **18**. The solution, which immediately turned purple, was stirred at room temperature for 4 h. Subsequent oxidation of the resulting anion with *p*-chloranil yielded the (*trans*)-4-ferrocenylvinylene-2,3,5,6-tetrachlorophenyl-bis(pentachlorophenyl) methyl radical (**1**), after chromatographic purification (silica gel and *n*-hexane/CCl_4; 1:1) and recrystallization from C_6H_6 with a 83% yield. This radical is completely stable in air both in the solid state and in dilute solutions. Remarkably, the resulting radical species retained the *trans* configuration of its precursor species in spite of the use of a strong base as an oxidizing agent. Single crystals of **1** for the X-ray structure analysis were grown by slow evaporation from methylene chloride/ hexanes (1/1) mixture (see Crystallographic Data, Chapter 6).

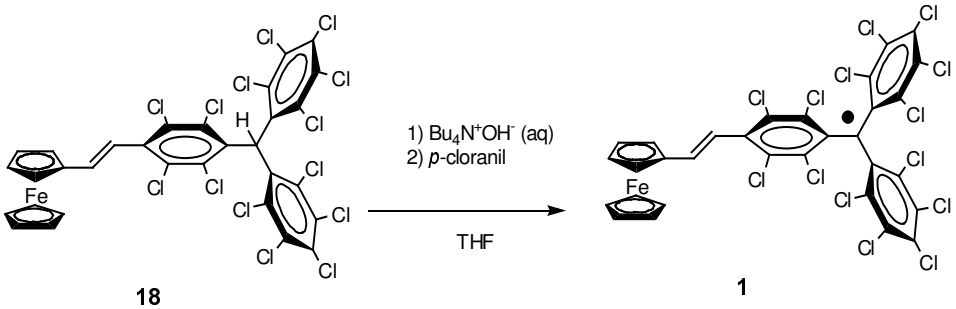

Scheme 8

2.2.3 Synthesis of (*trans*)-4-nonamethylferrocenylvinylene-2,3,5,6-tetrachlorophenyl-bis(pentachlorophenyl) methyl Radical 2

Initially, the synthesis of radical **2** was performed following the three synthetic steps previously described, i.e., synthesis of the substituted phosphonium bromide **17**, its corresponding Wittig reaction with the nonamethylated ferrocene carboxaldehyde derivative and sequent deprotonation and oxidation to yield the desired radical. However, even though the desired radical was obtained, the yield was remarkable small (<10%) probably due to the deactivation of the carboxydehyde group by the higher electron donor substituents present in the nonamethylferrocenecarboxadehyde **19**.

To improve the yield of radical **2**, a synthetic variation based on the use of a *Wittig-Horner-Emmons reaction* instead of the classical *Wittig reaction* was used. The *Wittig-Horner-Emmons reaction* consists in the condensation of a phosphonate derivative with an aldehyde or ketone group. Such reaction is not stereoselective, fact that may induce the formation of both, *trans* and *cis* isomers. Then, the synthetic route to prepare radical **2** is based on three main steps: I) synthesis of the substituted phosphonate **20**,[12] II) *Wittig-Horner-Emmons* reaction between the corresponding ferrocene carboxaldehyde derivative and the phosphonate **20** and III) sequent deprotonation and oxidation to yield the desired radical.

*I) Synthesis of the substituted phosphonate **20***

The substituted phosphonate **20** was obtained by an Arbuzov reaction with the bromomethane derivative **16** and an excess of triethylphosphite (Scheme 9), as previously described.[7,12]

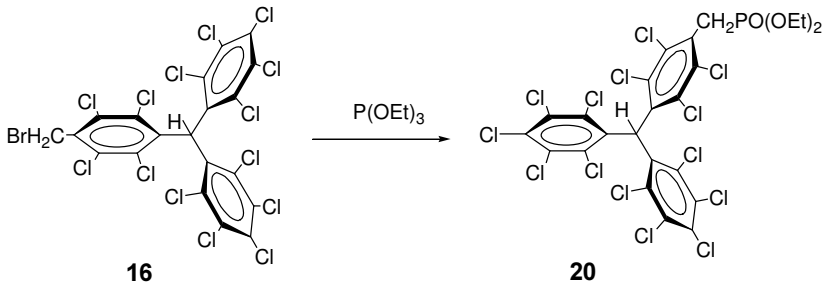

Scheme 9

II) Wittig-Horner-Emmons reaction

The reaction of **20** with the nonamethylferrocenealdehyde in the presence of potassium *tert*-butoxide is not stereoselective yielding, as expected, a mixture of the *trans* and *cis* isomers. Nevertheless, probably due to the high steric hindrance of the nonamethylated ferrocene and the perchlorinated rings of the triarylmethane unit, the isomer *cis*-**21** is obtained in a very low yield (< 2%), reason why exclusively the *trans* isomer was isolated and characterized.

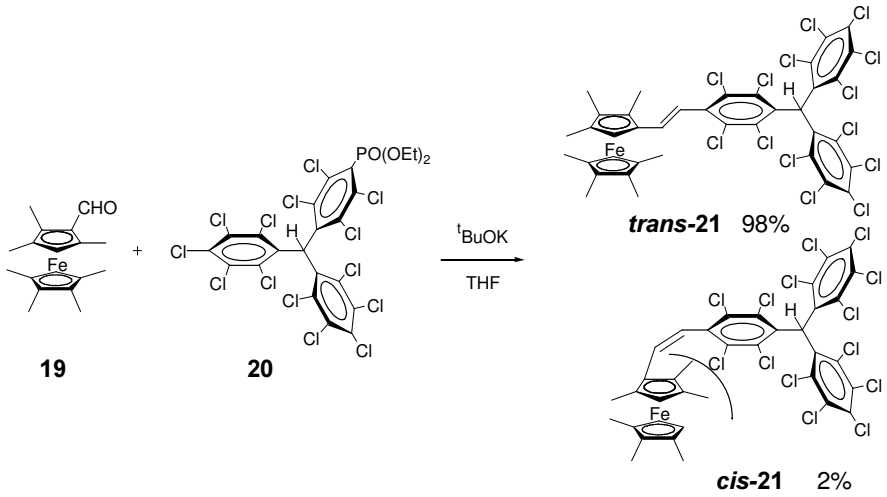

Scheme 10

To fully confirm that the microcrystalline material obtained was the isomer *trans*-**21,** additional ^{1}H-NMR experiments were carried out. As shown in Figure 7, ^{1}H-NMR spectrum of a solution of **21** exhibits three different kind of signals assigned to three different kinds of hydrogens. The three different kinds of hydrogen present in the methyl substitutents of the ferrocene are, a, b and c and appear to be in 1.69, 1,79 and 1,94ppm. The three singlets integrate 6, 6 and 15 hydrogen for b, c and a groups, respectively. The α-hydrogen appears at much lower field, 7.05ppm, due to its highly electron withdrawing surrounding. The hydrogens of the vinylene double bond appear as two doublets at 6.96ppm and 6.69ppm with the typical *trans* coupling constants of 16.6Hz for both of them (Protons d and e, Figure 7).

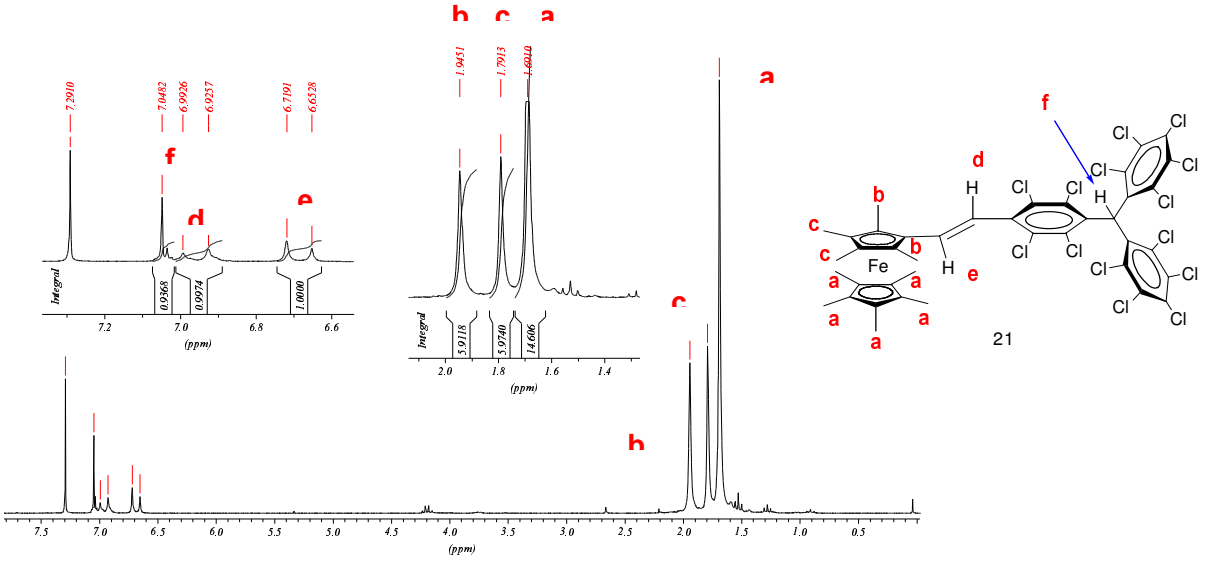

Figure 7. ^{1}H-NMR of *trans*-**21** with proton assignments.

III) Deprotonation and oxidation

The third step involves a deprotonation process and subsequent oxidation of the resulting anion to generate the corresponding radical species. Treatment of the triphenylmethane precursor **21** with an excess of KOH and (18-Crown-6) leads to the corresponding triphenylmethyl anion **22**, which has been isolated and fully characterized. Finally, the synthesis of the monoradical **2** was undertaken by oxidizing the triphenylmethylanion precursor **22** with $AgBF_4$ in dichloromethane. It is worth noting that the direct *one-pot* deprotonation and subsequent oxidation procedure used before for the generation of radical **1** here is not a good choice. This is because the *p*-chloroanil oxidant is in the case of compound **22** able to oxidize not just the anion to the radical species but also the ferrocene to ferrocenium species since the electron donating substituents of the methylated ferrocenyl compound **21** lower the oxidation potential with respect to that of the non-methylated ferrocenyl compound **18**. In order to avoid such non-desiderate oxidation another oxidant agent with a lower oxidation potential such as $AgBF_4$ have been used. In this case, the deprotonation and oxidation processes have to be performed in two different steps with the isolation of the precursor anion **22**. $AgBF_4$ is a very clean oxidation agent since silver (0) precipitate and it is easily separated form the reaction product by a simple filtration with a yield of 70% of **2**.

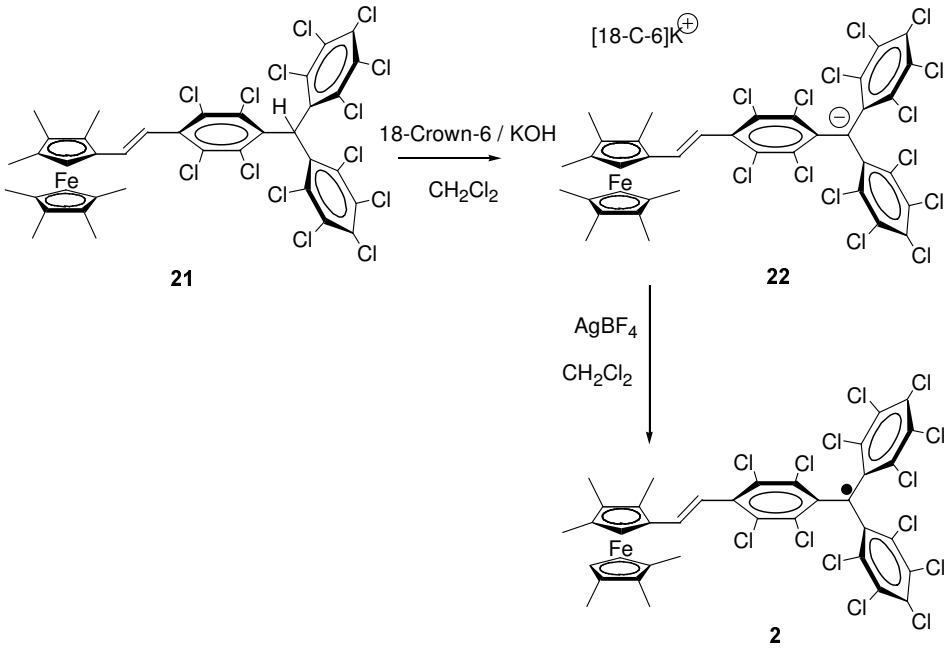

Scheme 11

2.3 SYNTHESIS OF METALLOCENE-BASED POLYRADICALS 7-10

2.3.1 Synthesis of (*trans-trans*)-1,1'-divinylferrocene-bis-[2,3,5,6-tetrachlorophenyl-bis(pentachlorophenyl)methyl] diradical (7) and (*trans-trans*)-1,1'-divinylruthenocene-bis-[2,3,5,6-tetrachloro phenyl-bis(pentachlorophenyl)methyl] diradical (9)

Analogously to the synthesis of the related ferrocene-based monoradical **3**, the synthetic route to prepare biradicals **7** and **9** involves the Wittig reaction between the corresponding ferrocene or ruthenocene biscarboxaldehyde derivative and the phosphonium bromide precursor **17** and the sequent deprotonation and oxidation to yield the desired biradical with a 45% yield for the ferrocene biradical **7** and 86% yield for the ruthenocene biradical **9**. The Wittig reaction between the phosphonium bromide precursor **17** and the ferrocene biscarboxaldehyde derivative is highly stereoselective (see Scheme 12), giving exclusively the *trans* isomer.[9] Remarkably, the resulting radical species retained the *trans* configuration of its precursor

.

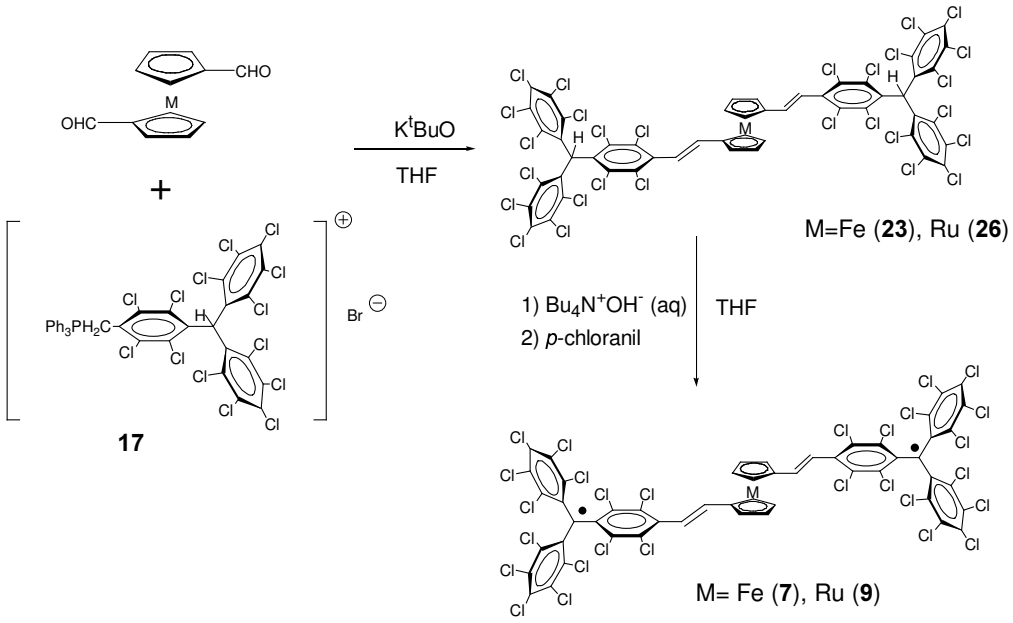

Scheme 12

2.3.2 Synthesis of (*trans,trans*)-1,1'-divinyloctamethylferrocene-bis-[2,3,5,6-tetrachlorophenyl-bis(pentachlorophenyl)methyl] diradical (8)

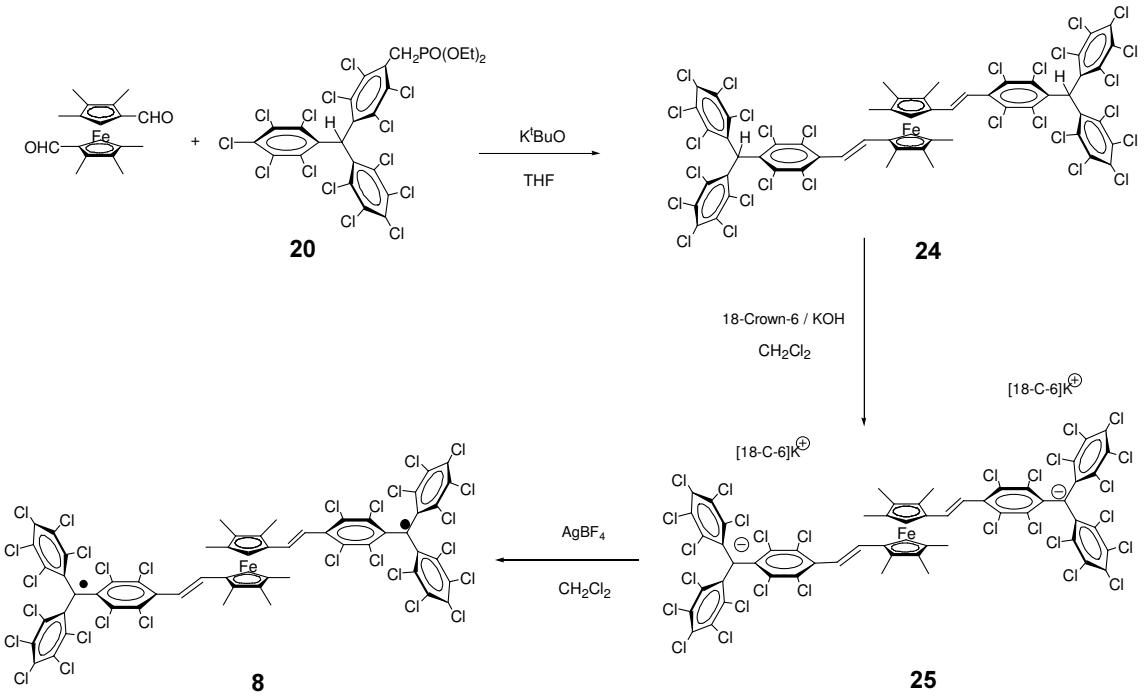

Scheme 13

The synthesis of biradical **8** was done following the same methodology than that previously described for analogous ferrocene-based monoradical **2**, which involves the *Wittig-Horner-Emmons* reaction between the corresponding ferrocene biscarboxaldehyde derivative and the phosphonate **20** and the sequent deprotonation and oxidation of the obtained bistriphenylmethane derivative to yield the desired diradical (30% yield). The synthesis of the precursor phosphonate **20** was previously described. As previously described for the monoradical **2**, the *Wittig-Horner-Emmons* reaction turned out to yield almost exclusively the *trans-trans* isomer (see Scheme 13). Remarkably, the resulting radical species retained the *trans-trans* configuration of its hydrogenated precursor.

For the characterization of all these polychlorotriphenylmethyl compounds different techniques have been used (see Experimental Part, Chapter 5) but it is worth noting the mass spectrometry measurements which have been performed using the LDI-TOF (Laser Desorption Ionization-Time of Flight) technique. This technique is specially used for sensitive molecules with high molecular weights.

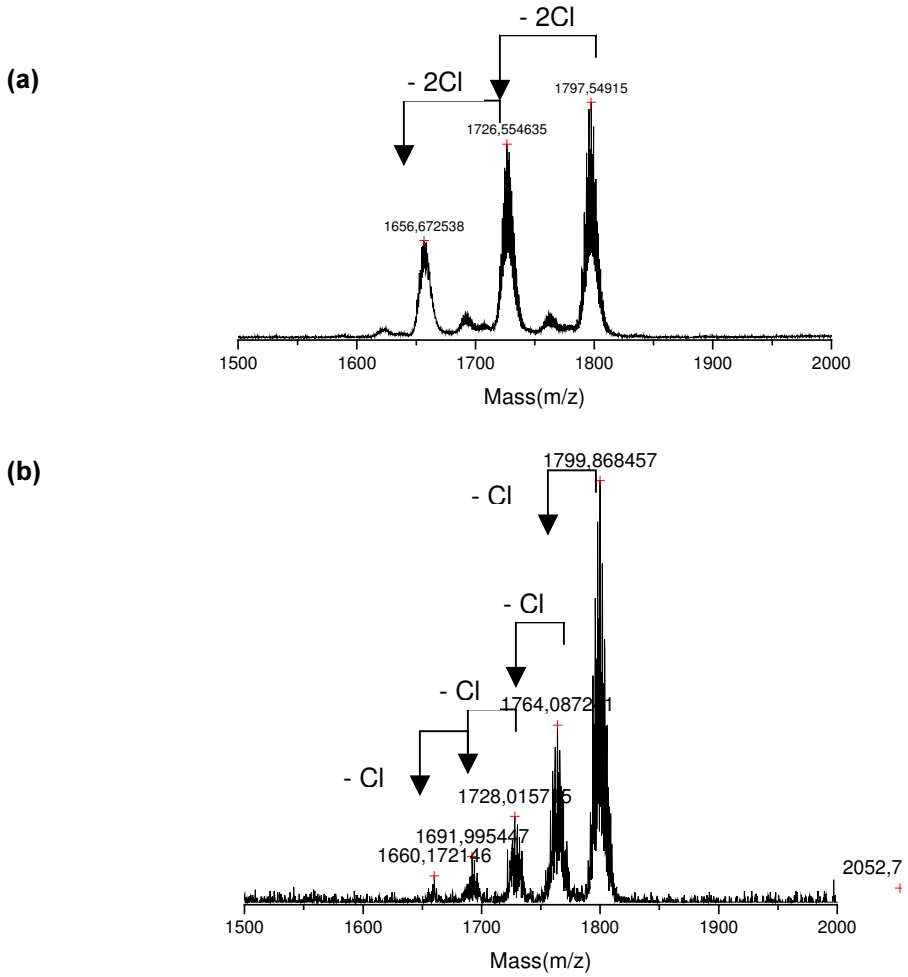

Figure 8. Mass spectra of the diradical **8** (a) and the correspondent bis α-protonated **24** (b)

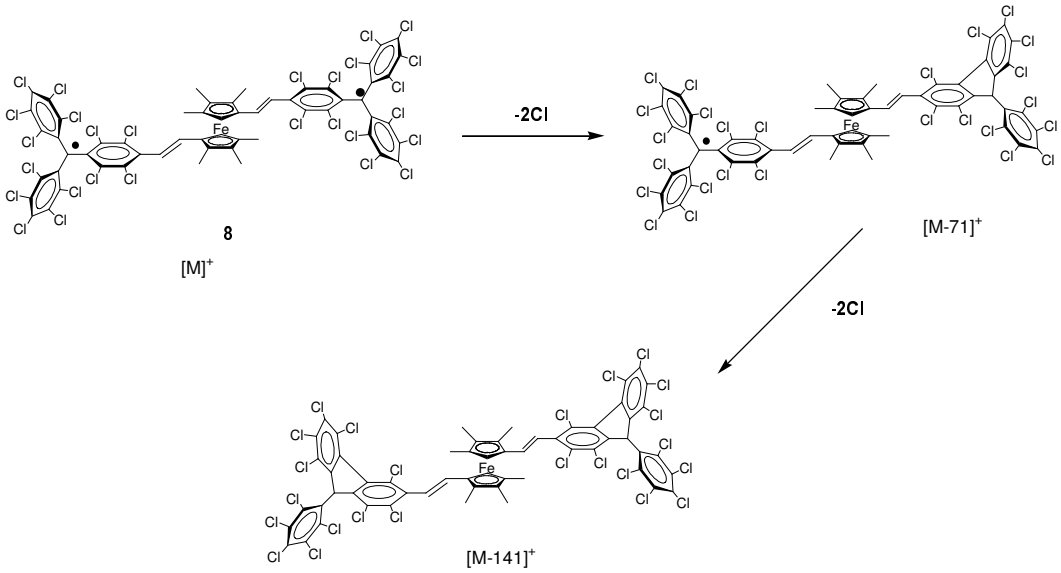

Figure 9. Degradation of the diradical **8** by generation of the correspondent mono- and bis- fluorenyl.

Due to space limitation it is not possible to present the mass spectra for all these compounds but here we will just present one example of it. Most of the LDI-TOF mass spectra for polychlorotriphenylmethyl compounds are very clean and very regular with the presence of the molecular peak $[M]^+$ and peaks separated by 35 units mass/charge. This result is totally coherent with the triarylmethyl radicals with chlorines in the *ortho*- positions, which degradate photochemically loosing two chlorine atoms to give the corresponding fluorenil species, which are more stable (Figure 9).[13] That's the reason why the most intense peaks correspond to the loose of two chlorines for this family of radicals (Figure 8a). We don't observe the same for the α-protonated precursors of the radicals. These species are not so instable and the loose of two chlorines at the same time takes place once at each time (Figure 8b).

As it is observed in all spectra, all peaks present the characteristic isotopic distribution associated to the presence of chlorines atoms. By simulating such distributions it is possible to know exactly the number of chlorine atoms for each peak. As the number of chlorines diminish, the resolution of the peaks increase.

2.3.3 Synthesis of (*trans,trans,trans*)-1,3,1'-trivinylruthenocene-tris-[2,3,5,6-tetrachlorophenyl]bis(pentachlorophenyl)] triradical (10)

The synthetic route used to prepare triradical **10** is the same one used for diradical **8** that is a Wittig reaction between the corresponding ruthenocene triscarboxaldehyde derivative and the phosphonium bromide precursor **17** and sequent deprotonation and oxidation to yield the desired triradical with a 35% yield. The Wittig reaction between the phosphonium bromide precursor **17** and the ruthenocene triscarboxaldehyde derivative is highly stereoselective, yielding exclusively the *trans* isomer.[8] (see Scheme 14). Remarkably, the resulting radical species retained the *trans* configuration of its precursor in spite of the use of a strong base as an oxidizing agent.

One of the techniques most used for the characterization of all these polychlorotriphenylmethyl compounds is the UV-Vis/Near IR spectroscopy. UV-Vis-NIR spectra offer the possibility to compare qualitatively predictions based upon the effect of the donor strength by changing iron for ruthenium, varying degrees of methylation of the cycloplentadienyl rings and also by changing the number of radical substituents for each metallocene. The visible spectra for polychlorotriphenyl methyl radicals (PTM) show an intense absorption band at around 358nm, which is assigned to the radical character of the triphenylmethyl unit.[14] Polychlorinated triphenylmethyl units connected to a metallocene, owing to the presence of more degrees of intramolecular electron transfer, present different absorptivities, and bathochromic shifts compared with unsubstituted chlorinated triarylmethyl radicals, as would be expected (see Table 1).

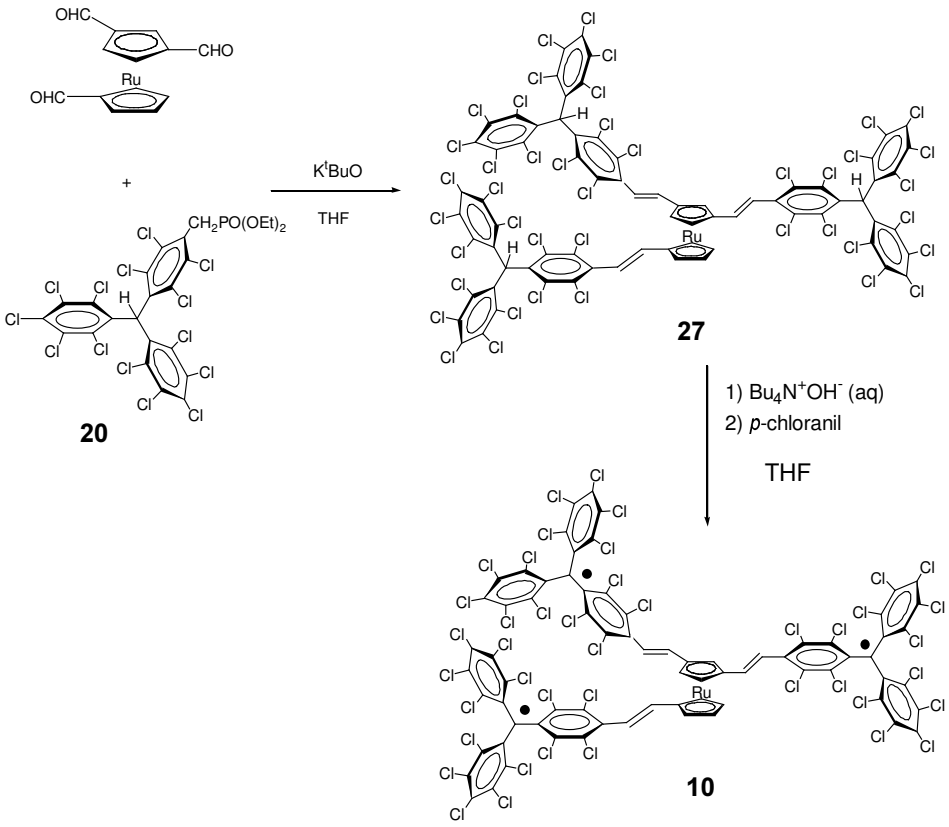

Scheme 14

Table 1. Relevant UV/Vis-NIR Data measured in CH_2Cl_2

Compound	λ_{rad} (nm)	ε ($M^{-1}cm^{-1}$)	λ_{IET} (nm)	ε ($M^{-1}cm^{-1}$)
PTM	358	32338		
1	386	26500	936	848
7	387	44880	920	1980
2	385	11400	1477	965
8	386	20937	822	686
9	387	50575	696	3500
10	387	72290	675	4706

When the number of radical units connected to a metallocene increases, an increase of the absorption values for the radical band is observed. It is also worth noting that when the donor ability of the ferrocene is enhanced, as in the case of methyl cyclopenadiene units,

the radical signal. This is an indication of the higher degree of intramolecular electron transfer for these compounds in solution so lower absorption bands associated to the radical character for these compounds are observed. The degree of intramolecular electron transfer also decrease with decreasing of the strength of the donor unit. For instance when the ferrocene is substituted for the ruthenocene, which has less donor ability and so less degree of electronic coupling with the radical centers**.** The radical character of the compound increases and the absorption of the radical band also increases. Also noteworthy is the dramatic increase in the intensity of the low energy transition when iron is exchanged for ruthenium. One reason is presumable the increased d-orbital extent of ruthenium, leading to increase direct or indirectly spatial overlap with the acceptor radical unit.

Characterization by other techniques such as elemental analysis, HPLC, cyclic voltammetry, FT-IR and ESR spectroscopy of all the compounds described in this section are described in the Experimental Part (see Chapter 5) of this thesis.

REFERENCES

1. Ballester, M.; Riera, J. Castañer, J.; Badía, C.; Monsó, J. M. *J. Am. Chem. Soc*. **1971**, *93*, 2215.
2. Ballester, M.; Riera, J.; Castañer, J.; Rovira, C., Armet, O. *Synthesis,* **1986**, 64
3. Armet, O.; Veciana, J.; Rovira, C.; Riera, J.; Castañer, J; Molins, E.; Rius, J.; Miravitlles, C.; Olivella, S.; Brichfeus, J., *J. Am. Chem. Soc.* **1987**, *91*, 5608
4. Fox, M. A.; Gaillard, E. Chen. C.-C., *J. Am. Chem. Soc*. **1987**, *109*, 7092
5. Teruel, L.; Viadel, Ll.; Carilla, J.; Fagarí, Ll.; Brillas, E.; Sañé, J.; Rius, J.; Julià, L. *J. Org. Chem*. **1996**, *61,* 6063.
6. Ballester, M.; Veciana, J.; Riera, J.; Castañer, J.; Rovira, C.; Armet, O., *J. Org. Chem*. **1986**, *51*, 2472
7. Rovira, C.; Ruiz- Molina, D.; Elsner, O.; Vidal-Gancedo, J.; Bonvoisin, J.; Launay, J.-P.; Veciana, V., *Chem. Eur. J.,* **2001**, *7*, 240.
8. For other strongly trans-selective reactions, see for example: Pommer, H.; Nurenbach, A., *Angew. Chem.* **1977**, *89*, 437; *Angew. Chem. Int. Ed. Engl.* **1977**, *16,* 423.
9. House, H. O.; *Modern Synthetic Reactions*, 2nd ed., Benjamin, Menlo Park, **1972**, p. 608.
10. a) Wurst, K.; Elsner, O.; Schottenberger, H., *Synlett*, **1995**, 833 b) Rodriguez, J.-G.; Oñate, A.; Martin-Villamil, R. M.; Fonseca, I., *J. Organomet.Chem*., **1996**, *513*, 71
11. Fitjer, L.; Quabeck, U., *Synth. Commun*., **1985**, *15*, 855.
12. For a review see: Stec, J*., Acc. Chem. Res*, **1983**, *16*, 411
13. Fox, M. A.; Gaillard, Chen, C. C.; *J. Am. Chem.. Soc*. **1987**, *109*, 1961.
14. Ballester, M.; Riera, J.; Castañer, J.; Rodríguez, A., *Tetrahedron Lett.,* **1971**, 2079; (b) Ballester, M.; Riera, J.; Catañer, J.; VecianaJ.; Rovira, C., *J. Org. Chem.* **1982**, *47*, 4498.

3 | RESULTS

3.1 | Magnetism

3.2 | Electronic Properties

3.3 | Nonlinear Optical Properties

3.1 Magnetism

3.1.1 INTRODUCTION

Due to the light nature of elements composing organic compounds, only the magnetic exchange interactions determine the magnetic behavior at temperatures well above 0.1 K.[1] Other kinds of magnetic interactions (such as hyperfine, dipolar or spin-orbit interactions) can be considered as negligible above this temperature in most organic materials. Consequently, magnetic organic systems may be described at zero applied magnetic field by the effective spin Hamiltonian approach that takes the form,

$$H = -2\Sigma J_{ij}\, \mathbf{S}_i \cdot \mathbf{S}_j \qquad \textbf{Equation 1}$$

where J_{ij} represents the effective exchange interaction parameter for magnetic centers i and j (the spin-containing building blocks) which have total quantum spin numbers S_i and S_j, respectively, and the summation runs over all the adjacent pairs of centers. The J_{ij} parameter is a scalar constant, which is often referred as the isotropic interaction parameter or exchange coupling constant between the two interacting magnetic centers. This constant describes the isotropic part of the magnetic interaction that occurs through bonds –either covalent or non-covalent (H-bonds, π-π interactions, etc)– and leads to a splitting between a pair of states. In fact, J_{ij} is related with the energy separation of the two states of an ideal system formed by just these two i and j centers. When J_{ij} is positive the two spins tend to be parallel to each other in the ground state and the interaction (or coupling) is called ferromagnetic. If J_{ij} is negative the two spins tend to be antiparallel in the ground state and the interaction is called antiferromagnetic.

Most organic magnetic materials exhibit paramagnetic behavior at high temperatures where the spins of the material behave independently of each other. However, as the temperature is decreased, the exchange interactions become comparable with the thermal energy of the system and the neighbouring spins tend to align in accordance with the signs of their J_{ij} parameters. Under these conditions, the spin ordering is propagated within small regions of the material and a short-range order is attained. This short-range ordering can be propagated locally (as for discrete clusters) or in one (for regular chains), two (for sheets), or three dimensions, depending on the relative magnitudes of J_{ij} in the three directions of the solid material. Under these circumstances, the spin ordering is propagated throughout the three dimensions of the material and a long-range magnetic ordering might be achieved.

However, in most spin-containing organic molecules, the spins are regarded as being of the Heisenberg type, that behave nearly isotropically. One of the most important consequences of this fact is that the exchange interaction between them only fixes the relative orientation of the spins but does not promote any preferential orientation (or direction) of the interacting spins with respect to the atomic framework of the material since the energy of all possible directions are nearly identical. A preferred direction for the spin alignment in an organic magnetic material is only achieved if a source of magnetic anisotropy is present in the material. In purely organic compounds the two main sources of anisotropy are spin-orbit couplings and magnetic dipolar interactions that generally have a small magnitude. In spite of this fact the last type of anisotropy might become effective for materials with low magnetic dimensionalities; i.e. materials in which the exchange interactions are propagated in one (regular chains) or two dimensions. Magnetic anisotropy might also be introduced if a transition metal forms part of the molecules, as occurs in metal-organic compounds and networks, because of the single-site anisotropy of such atoms.

Keeping on mind the characteristics previously described, the design and development of organic molecular materials showing interesting magnetic properties involves two main aspects or steps: I) the spin containing building blocks and II) their coupling routes (mechanisms).

3.1.1.1 Spin Containing Building Blocks

Most organic open-shell molecules are reactive intermediates formed along different reactions such as homolysis, free radical addition or electron transfer reactions. In spite of such instability, the magnetic properties of different radical series, whose persistence varies depending on their nature, topology and structure, have been reported. Such families of radicals include α-nitronyl nitroxides, galvinoxyls, semiquinones and triarylmethyl radicals, among others. To increase their stability kinetically and, to some extent, thermodynamically, there are two main general strategies. One of the most efficient methods for raising the persistence of free radicals is the increasing of the steric shielding of atoms having large unpaired electron densities. The idea behind this method is to protect effectively these centers with bulky substituents from attack by other reactive molecules present in the surroundings. Using this idea different kinds of highly persistent free radicals have been reported (see Scheme 15).

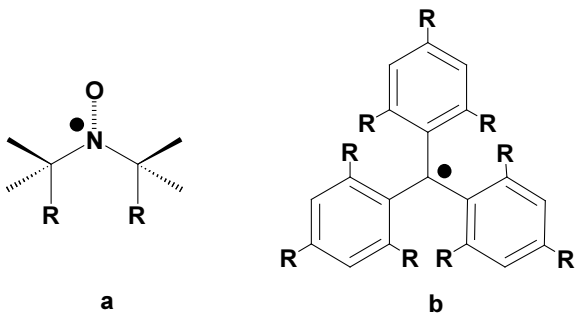

a b

Scheme 15

For instance, methyl substituents at the α positions of substituted aminoxyl radicals shield sterically the NO group where the unpaired electron is mainly localized hindering the approach of any reactant (Scheme15-a). Other examples of highly persistent species are the highly substituted triphenylmethyl radicals which show outstanding chemical and thermal stabilities that are also traced predominantly to the shielding of their trivalent carbon atoms (Scheme15-b). The main disadvantage of using large groups to increase the life expectancy of organic radicals is the decrease of intermolecular interactions; i.e., the larger the substituents the lower the chances of each site to interact magnetically with its neighbors. Actually, most of the radicals with bulky substituents show quasi-ideal paramagnetic behaviors evidencing the insignificance of intermolecular magnetic interactions.

The second main strategy to increase the persistence of an open-shell organic compound is to replace the carbon radical center with an heteroatom: namely, the use of heteroatom-centered radicals (see Scheme16). Due to the electronegativity of the spin centers, the spin density is more localized at the heteroatom, thereby facilitating the steric protection. Indeed, since the bond connecting the heteroatoms directly is thermodynamically less stable than carbon-carbon bonds, the merit of recombination reactions is attenuated.

The third strategy is to increase the electronic localization of the unpaired electron.

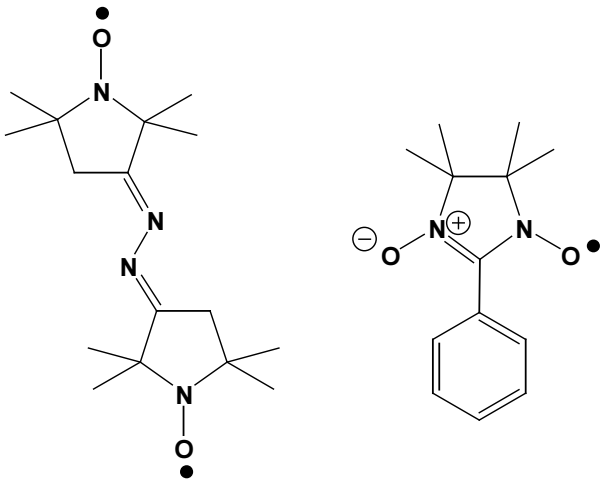

Scheme 16

Polychlorotriphenylmethyl radicals used in the present thesis are open-shell organic units that have their unpaired electrons delocalized in three aromatic rings and also they have their open-shell centers (or trivalent carbon atoms) sterically shielded by an encapsulation with six bulky chlorine atoms in order to increase their life expectancies and thermal and chemical stabilities. For instance, it is very well known that the monoradical counterpart, the perchlorotriphenyl methyl radical shows an astonishing thermal and chemical stability for which the term of inert free radical was coined.

3.1.1.2 Coupling Routes

There are two complementary approaches to prepare organic magnets depending on whether the magnetic interactions that allow the electron spins of the constituent free radicals to align are *intermolecular* or *intramolecular*. In both cases, a ferromagnetic interaction results if an orthogonal arrangement of SOMO's, with a null overall overlap integral between such orbitals is produced. On the other hand, if such an integral is non-zero, the resulting magnetic interaction would be antiferromagnetic for non-degenerate orbitals. A paradigmatic example of an organic molecule showing a ferromagnetic coupling produced by the potential exchange term is diphenylcarbene in which intrinsic orthogonality of the two SOMO's, containing the two unpaired electrons, exists (see Figure 10) because of their s and p symmetries.[2,3]

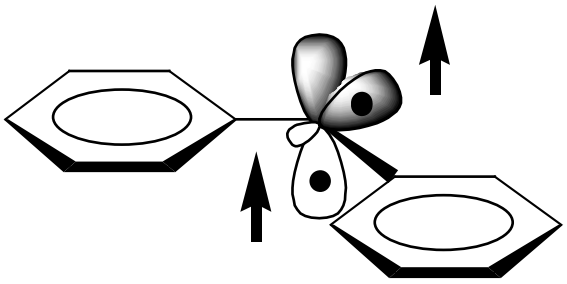

Figure 10. Simplified scheme of the singly occupied molecular orbitals (SOMOs) of diphenylcarbene, showing intramolecular ferromagnetic coupling of two spins.

1. *Intermolecular* interactions among organic radicals are mainly determined by the isotropic exchange interactions between unpaired electrons located on the singly occupied molecular orbitals (SOMOs) of the nearest-neighboring molecules. Depending upon the symmetry, degeneracy, and characteristics of the SOMO's and also on the mode of arrangement of the molecules in a crystal, the resulting interaction can align the spins in a parallel (ferromagnetic) or antiparallel (antiferromagnetic) manner. If the alignment occurs in the three dimensions of the material, then a long-range (or bulk) magnetization order, either ferro- of antiferromagnetic, may occur. In addition to ferromagnetic (FM) and antiferromagnetic (AFM) ordering, other types of long-range magnetic orderings such as weak (or canted) ferromagnetic (WFM) and/or ferrimagnetic (FIM) order can in principle also be achieved if the magnetic interactions are properly propagated throughout the crystals in three dimensions. The construction of such solids requires that the structural subunits exhibit non-covalent interactions suitable to be controlled in a predictable manner.

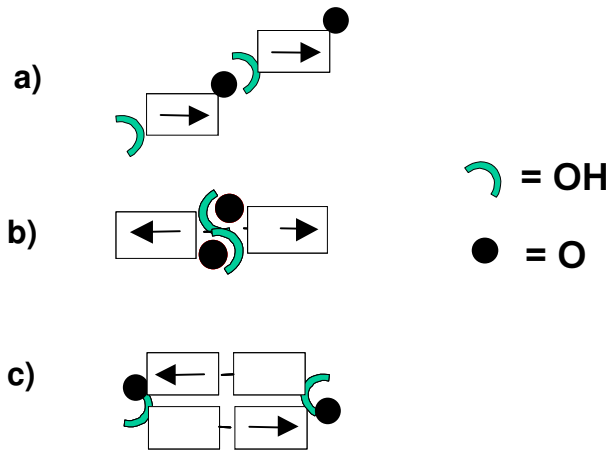

Figure 11. Schematic representation of different kinds of non-covalent interactions between spin-containing building blocks.

Up to now, the different types of non-covalent intermolecular interactions that have been used for the assembly of such molecular subunits are hydrogen-bonding, transition-metal ligation, stack-type alignment and bridging of ion radicals by their counterions. Among them, hydrogen-bonding has emerged as a particularly useful and efficient tool. Indeed, transmission of magnetic interactions through hydrogen bonds was first observed with transition metal complexes. Since then, several hydrogen-bonded organic magnets have been reported.

Representative examples of organic molecular crystals exhibiting FM order are the β-phases of *o*-hydroxyphenylnitronyl aminoxyl radical and the bis(aminoxyl)adamantane diradical (Figure12).

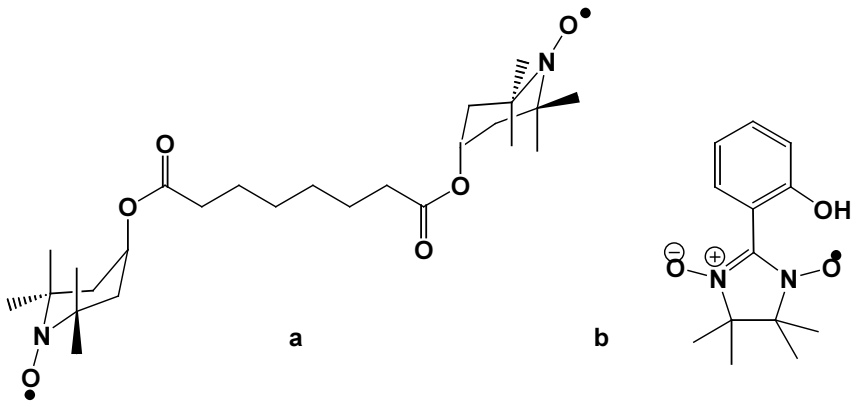

Figure 12. Bis(aminoxyl)adamantane diradical **a** and the β–phases of *o*-hydroxyphenylnitronyl aminoxyl radical **b**

2. *Intramolecular* interactions are also due to exchange interactions. Thus, when a molecule has two high-lying orthogonal orbitals, close or equal in energy, with two less electrons than necessary for a closed shell structure, its ground state becomes triplet as dictated by Hund's rule. However, the actual nature of the interaction (FM or AFM) depends upon the symmetry and topology of the degenerate or nearly degenerate SOMO's orbitals. One of the general approaches to obtain high-spin organic compounds is based on conjugated polyradicals with topologically polarized π–spins. These compounds are designed using an appropriate ferromagnetic coupling unit able to align in parallel the electron spins of a pair (or triad) of radical centers connected through such a unit.[4]

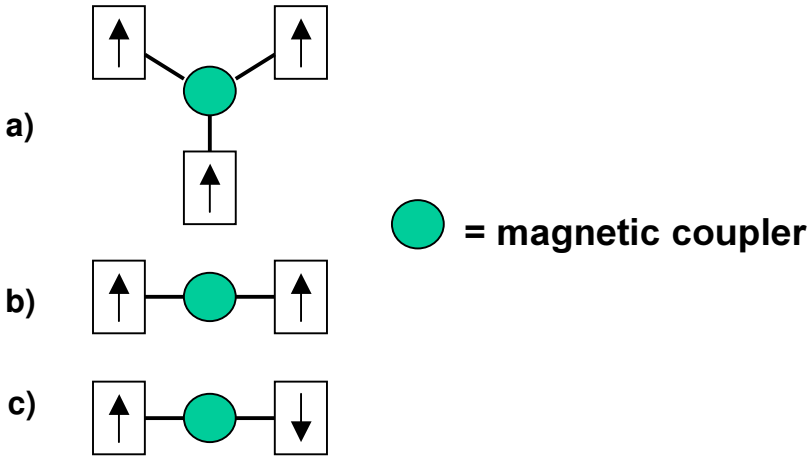

Figure 13. Schematic representation of spin-containing building blocks with parallel or anitparallel alignment of the pair or triad of radical centers connected through a magnetic coupler

m-Phenylene has become the most widely used ferromagnetic organic coupler because it is highly dependable. Thus, this unit is able to couple ferromagnetically not only carbon- and nitrogen-centered free radicals but also carbenes, nitrenes, and polarons.[5] In addition, *m*-phenylene couplers can be modified with a large variety of substituents without changing the robust spin preference dictated by the topology rules,[6] except for few cases where a large torsion angle between the nodal plane of the π-spin source and the coupler unit plane is induced.[7]

Efforts to increase the number of the aligned spins using 1,3-phenylene couplers have been disturbed by the presence of spin defects and/or bond distortions, which have been shown to affect the ferromagnetic exchange coupling through *m*-phenylenes. To overcome such problems, other complementary approaches such as the use of π-conjugated linear polymers bearing pendant radical groups, π -conjugated polycyclic polymers with alternative coupling pathways, or the use of diamagnetic metal ions as ferromagnetic couplers have been used.[8]

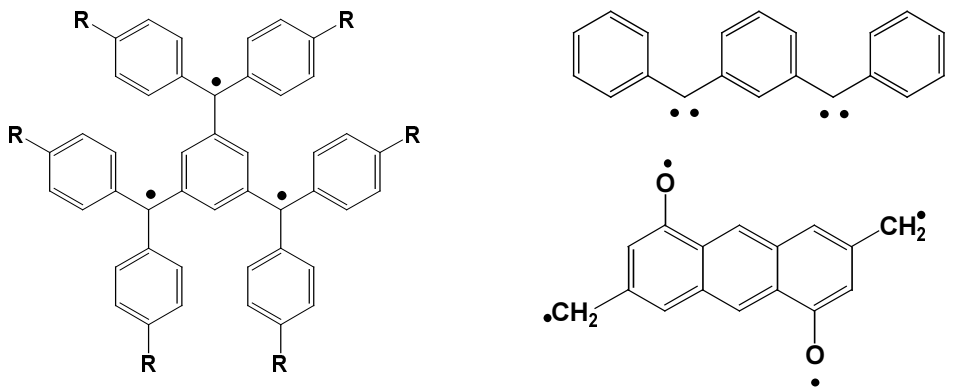

Figure 14. Topological degeneracy using *m*-phenylene couplers

In our group, we focused our attention in the development and study of new magnetic coupler units, more precisely metallocene (ferrocene and ruthenocene) units, able to promote ferromagnetic interactions between pure organic radicals covalently linked to them (Scheme 17). Up to now it has only been used as building block of molecular solids promoting intermolecular magnetic interactions very successfully.

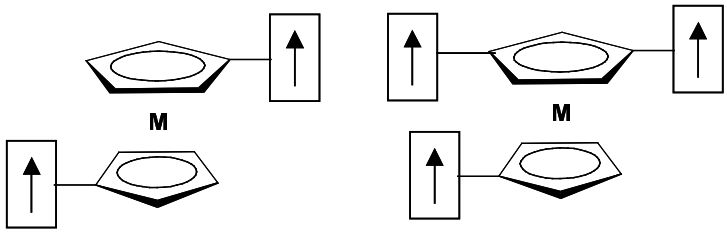

M=Fe, Ru

Scheme 17

3.1.2 RESULTS

In this chapter, the capability of polychlorotriphenylmethyl monoradicals **1**-**5** to generate supramolecular magnetic materials (exhibiting *intermolecular* magnetic exchange interactions) as well the capability of metallocene units to transmit magnetic interactions between polychlorotriphenylmethyl radicals in diradicals **7**-**10** (*intramolecular* magnetic exchange interactions) have been analyzed and the corresponding magnetic properties are described herein.

3.1.2.1 Supramolecular Magnetism (Intermolecular Interactions)

Solid state studies: The static magnetic susceptibility, χ, of polycrystalline samples of radical **1**-**5** were measured between 2 K and 300 K with a SQUID susceptometer under different external applied fields. Surprisingly, for radicals **1**-**4** the $\chi \cdot T$ product values at room temperature diverge from the theoretical value of 0.37 emu.K.mol^{-1} expected for uncorrelated S=1/2 systems. For instance, magnetization data for radical **1** collected under an external field of 1T is shown in Figure 15.

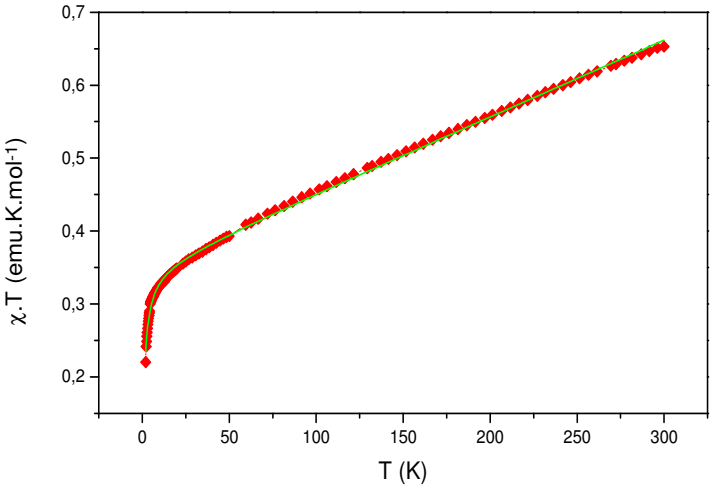

Figure 15. Temperature dependence of the magnetic susceptibility for radical **1** over the 5-293 K temperature range, in the of form χT vs. T.

The $\chi \cdot T$ versus T plot for radical **1** revealed that its $\chi \cdot T$ moment at 300 K was 0.65 emu.K.mol^{-1}, recurrent measurements giving similar $\chi \cdot T$ moment values. Such value is outsized to be justified in terms of an organic radical contribution, for which a theoretical value of 0.37 emu.K.mol^{-1} was expected. A decrease of the temperature reveals a steady decrease of $\chi \cdot T$ down to a value of 0.30 emu.K.mol^{-1} at 10 K, whereupon the $\chi \cdot T$ moment abruptly decreases probably due to the presence of intermolecular magnetic exchange interactions, as previously observed in related polychlorotriphenylmethyl radicals.[9] The outsized $\chi \cdot T$ value at room temperature and the steady decrease of the μ_{eff} moment between 300 and 10 K was assigned to significant spin-orbital contributions from a remnant $[Fe^{III}Cp_2]^+$ fraction present in the sample, which arises from a temperature-dependent intramolecular electron transfer phenomenon between the ferrocene and the radical units as depicted in Scheme 18 (for more details section Chapter 3.2). [10]

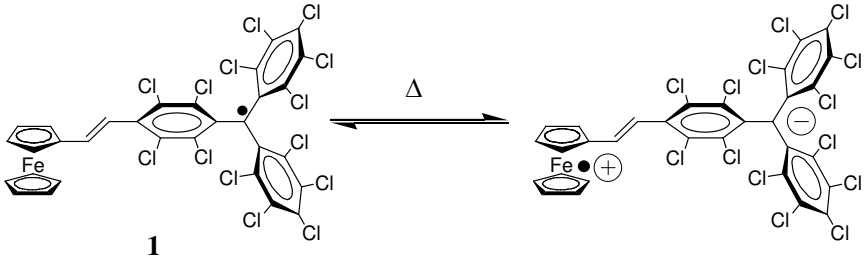

1

Scheme 18

It is also important to emphasize that the $\chi \cdot T$ plot is strongly field-dependent (see Figure 16), lower magnetic fields giving rise to more considerable deviations, or in other words, larger slops for the $\chi \cdot T$ plots. Such behavior may be tentatively attributed to distortions coming from spin-orbital contributions, although this option results difficult to justify from a magnetic point of view, or most likely, from field-induced variations on the intramolecular electron transfer process shown in Scheme 18 that originates an abrupt increase of the remnant $[Fe^{III}Cp_2]^+$ fraction. In any case, further work is currently underway to fully determine the origin for such strong field-dependent magnetic contribution.

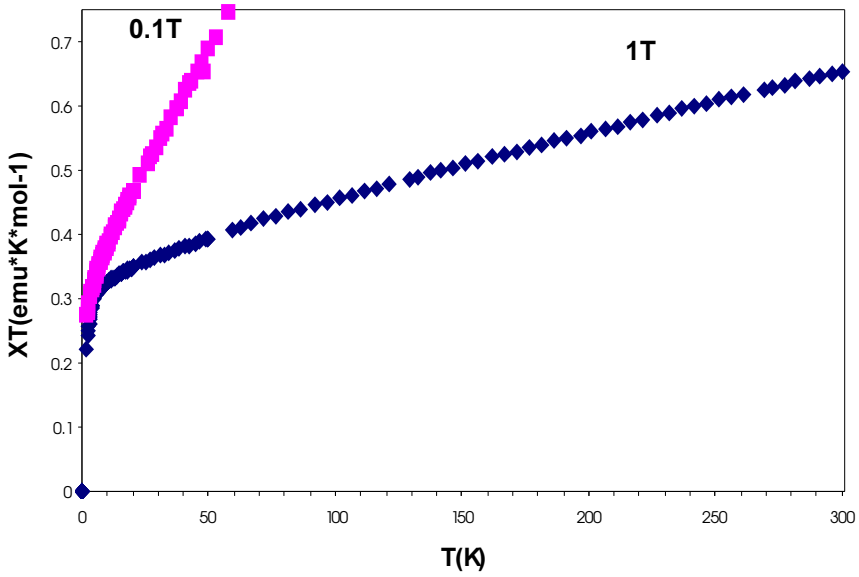

Figure 16. Temperature dependence of the magnetic susceptibilities for radical **1** over 4.2-300 K temperature range in the form χT vs. T at 0,1 and 1T.

Even though the observation of anomalously large $\chi \cdot T$ values was confirmed not only for radical **1** but also for radicals **2**-**4**, the magnetic susceptibility data for them was nicely fitted to the Curie-Weiss law, including an additional term accounting for the presence of temperature independent paramagnetism (TIP). The resulting effective magnetic moments and Weiss constants are shown in Table 2. The Curie values so far obtained are similar to those found for most polychlorotriphenylmethyl monoradicals up to now described. The Weiss constants for radicals **1**-**4** are negative and considerably small. This tendency is specific to this family of compounds, and could be explained by Cl···Cl and $\pi \cdots \pi$ interactions between aromatic rings of neighboring radicals, as these interactions are always present in their crystal structures. However, as can be observed on the same table, the main anomaly comes from the fit of the magnetic susceptibility data of radical **5** to a Curie-Weiss law, which yields an anomalous high Weiss constant of θ = -22.6 K.

Table 2. C, θ and TIP values found from the fit of the magnetic experimental data to the Curie-Weiss law for compounds **1**-**5**

Compound	C (emu.K.mol^{-1})	θ (K)	TIP (emu.mol^{-1})
1	0.36	-0.9	0.00105 [a] 0.00697[b]
2	0.36	-0.7	---[a] 0.00242[b]
3	0.36	-2.0	0.00832[a]
4	0.35	-2.1	0.00062[a]
5	0.39	-22.6	---[a]

[a] Measured with an external magnetic field of 1T ; [b] Measured with an external magnetic field of 0.1T

The question is: Why do the Weiss constant value found for radical **5** remains so different from that found for the related radical **3**? Tentatively, the stronger Weiss constant value found for radical **5** has been assigned to the presence of stronger intermolecular magnetic interactions in its solid state packing due to the formation of supramolecular dimeric species directed by intermolecular C-H···N hydrogen bonds between -CH=N- groups of two different molecules. The formation of such dimeric species is not expected to take place for radical **3** since its *trans* configuration will favor the presence of stronger steric congestions between the carbon atoms of the ferrocene group and the chlorine atoms of the triphenylmethyl group. In any case, the lack of an X-ray for radical **5** prevents us from knowing the precise disposition of molecules in the solid state. For this reason, the presence of relatively strong intermolecular magnetic interactions for compound **5** was confirmed by EPR experiments.

EPR solution studies: X-band EPR spectra of toluene/methylene chloride (1:1) solutions of radicals **1**-**5** ([c] = 10^{-5} mol.l^{-1}) were obtained in the temperature range of 160-300K. At 200 K, EPR spectra of radicals **1**-**4** show lines corresponding to the coupling of the unpaired electron with the different nuclei with non-zero magnetic moments ^{1}H, ^{14}N (if present) and naturally abundant ^{13}C isotopes at the α and aromatic positions. The isotropic hyperfine coupling constants (a_i) and the isotropic g-values (g_{iso}) found by computer simulation for radicals **1** and **3** are shown in Table 3. These values are similar to those previously described for related polychlorotriphenylmethyl radicals evidencing that both radicals exist in solution as monomeric species.

Table 3. EPR isotropic hyperfine coupling constants (a_i) and isotropic g-values (g_{iso}) of isotropic solutions of toluene/chloroform (1/1) solutions of radicals **1** and **3**.

		Hyperfine Coupling Constants (G)						
Compound	g_{iso}	**N**	$^{1}H_{meta}$	$^{1}H_{ethyl}$	$^{1}H_{ethyl}$	$^{13}C_{\alpha}$	$^{13}C_{ortho}$	$^{13}C_{bridge}$
1	2,0035	-	-	1.8	0.6	29,8	12,0	10,5
3	2,0030	1,2	1,1	-	0,3	28,5	12,5	10,3

More complicated resulted the EPR spectra of radicals **2** and **4**. Although such spectra exhibit lines corresponding to the coupling of the unpaired electron with the different nuclei with non-zero magnetic moments, the asymmetry of the resulting spectra make matters worse to their interpretation and therefore, to obtain the corresponding isotropic hyperfine coupling constants (a_i) and the isotropic g-values (g_{iso}). X-band EPR spectra of toluene/methylene chloride (1:1) solutions of radicals **2** and **4** ([c] = 10^{-5} mol.l^{-1}) obtained at 200 K are shown in Figure 17. The corresponding spectra of related non-methylated radicals **1** and **3** are also shown in the same figure for comparison purposes.

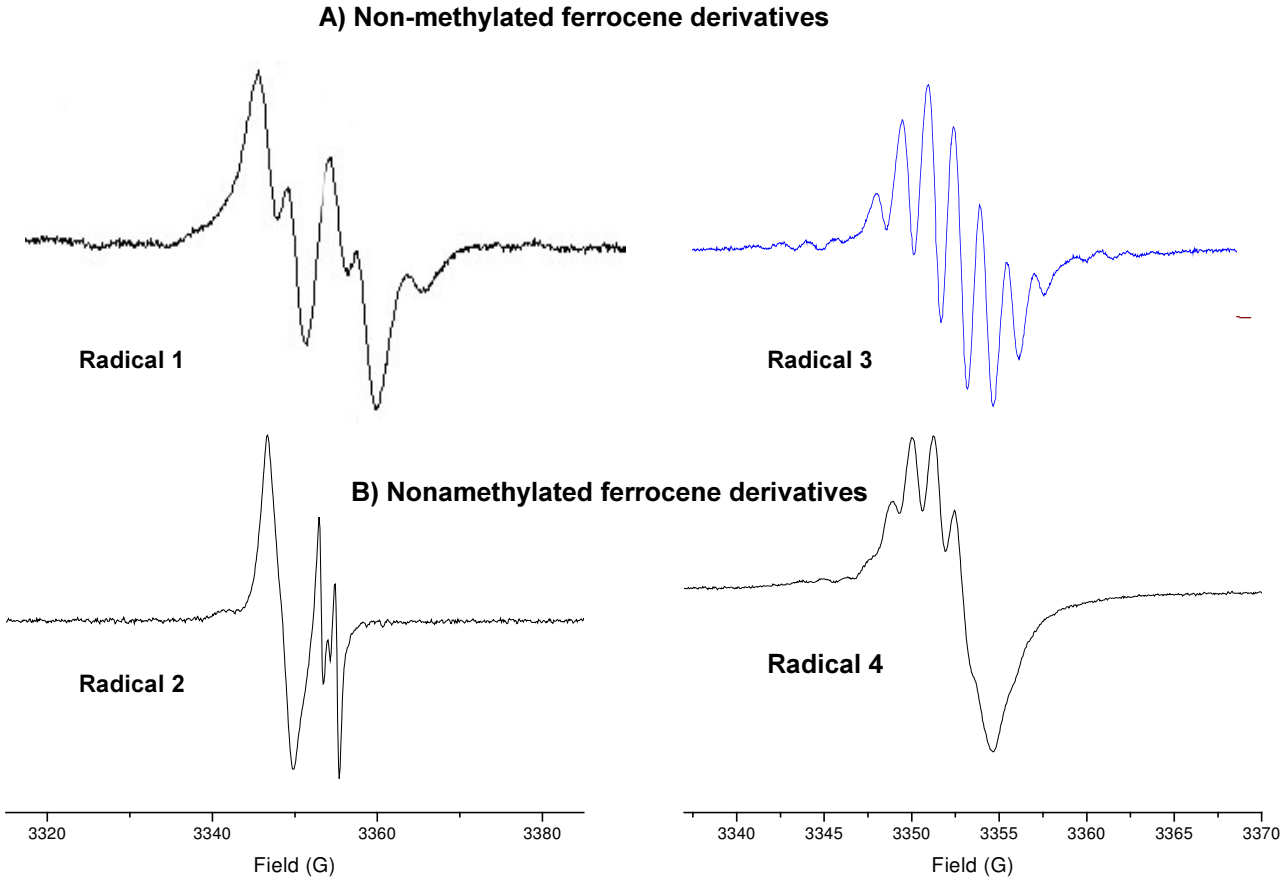

Figure 17. X-band EPR spectra of a toluene/CH_2Cl_2 solution of the non-methylated radicals **1, 3** and the nonamethylated ones **2** and **4** at 200 K

Such discrepancy has been tentatively attributed to an increase of the presence of the electronic isomer involving the ferricinium cation shown in Scheme 18 in radicals **2** and **4** with respect radicals **1** and **3** due to an increase of the donor ability of the methylated ferrocene units. Further studies to fully determine the origin of the asymmetry as well as the nature and values of the hyperfine coupling constants will be develop in a near future.

Even more intriguing resulted the X-band ESR isotropic spectrum of radical **5** obtained at 200 K, which does not provide any specific information about the lines

corresponding to the coupling of the unpaired electron with the different nuclei with nonzero magnetic moments but the characteristic fine structure of a triplet species (see Figure 18).

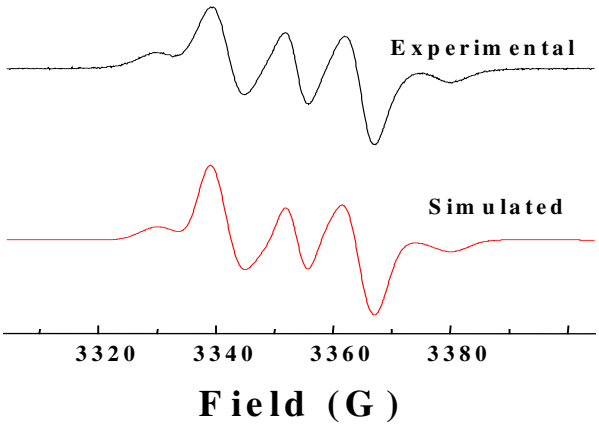

Figure 18. Experimental and simulated X-band EPR spectra of a toluene/CH_2Cl_2 solution of radical **5** at 220 K

The observation of a spectrum characteristic of a triplet species can be nicely explained by the formation of a supramolecular dimeric species directed by intermolecular C-H···N hydrogen bonds between -CH=N- groups of two different molecules (see Figure 19).

The study of the zero-field splitting parameters |D| and |E| confirmed the existence of a certain degree of electronic spin delocalization over the imino bridge that reduces the effective separation of the two spins in the diradical species, and therefore, will favour the presence of intermolecular magnetic exchange interactions. To confirm this possibility, the forbidden $\Delta m_s=\pm 2$ transition characteristic of triplet species was also observed at the half-field region of the spectrum and its intensity was measured in the 4-100 K temperature range. Such experiments showed that $I_{pp}T$ decreases with decreasing temperature indicating that the ground state of the dimeric species is the singlet state and the triplet state should be associated with a thermally accessible excited state. A separation of 54 ±2 K (38 cm^{-1}) between both states was obtained from the fitting of the experimental data to the Bleaney-Bowers equation (Papers III).

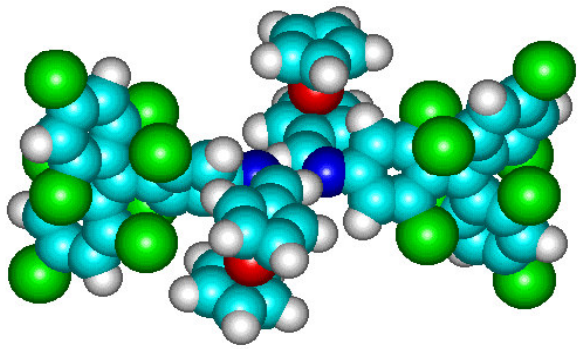

Figure 19. ZINDO/1 semiempirical optimized structure of the supramolecular hydrogen-bonded dimeric species of radical **5.**

Supramolecular Photomagnetic Switch

There is currently great interest in the obtaining of photomagnetic materials whose magnetic properties may be controlled at will by means of light.[11,12,13] Such control over magnetic properties by optical stimuli may have application in magneto-optical devices. Different examples of photoinduced magnetization changes in pure organic materials have been described so far.[14,15,16] For instance, photoisomerization of a carbene compound,[17] spin isomerization of a non-Kekulé diradical[18] or photoinduced interconversion of a photochromic singlet/triplet system. However, even though several examples of photomagnetic materials have been studied, to the best of our knowledge, there are no previous examples of supramolecular photomagnetic materials despite its enormous interest. The interconversion between radical *trans*-**3**, which exists in solution as a monomeric species, and its corresponding isomer radical *cis*-**5**, which aggregates in solution originating a hydrogen-bonded diradical species (*cis*-**5**)$_2$ with a singlet ground state which allowed us to establish for the first time a photomagnetic supramolecular system, shown in Scheme 19 (Papers I and II).

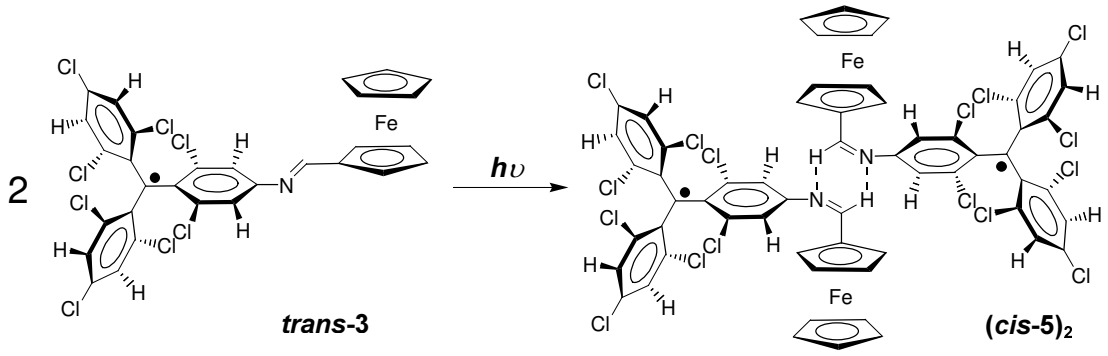

Scheme 19

Photoinduced experiments have been performed in collaboration with the Institut de Chemie de la Matiere Condense (CNRS) of Bordeaux under the supervision of Dr. J.-F. Létard. The photoinduced isomerization was monitored by ESR and UV-Vis spectroscopy at room temperature irradiating at 415, with an efficiency markedly dependent on the polarity of the solvent. Such dependence has been attributed simultaneous presence of *trans* to *cis* photoisomerization and intramolecular electron transfer processes, the latter being favored in the presence of polar solvents. For instance, radical **3** underwent photoisomerization in methylcyclohexane whereas irradiation in more polar solvents, such as methylene chloride or acetonitrile, which promote intramolecular electron transfer processes, does not originate any *trans-cis* isomerization process. As an example, the *trans*-**3** to *cis*-**5** photoinduced isomerization of a diluted solution of radical **3** in methylcyclohexane monitored by time-dependent EPR experiments is shown in Figure 20 (Paper I and X).

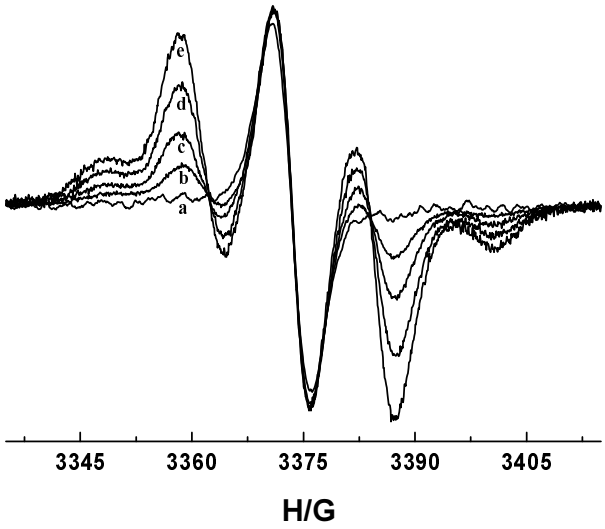

Figure 20. Photoinduced *trans-cis* isomerization of *trans*-**3** radical monitored by EPR spectroscopy at t = 0 (a), 1h (b), 3h (c), 5h (d) and 8h (e).

Finally, it must be emphasized that irradiation of a radical *cis*-**5** solution did not indicate the presence of the reverse photoisomerization process, either by EPR and/or by UV/Vis spectroscopy. Moreover, warming radical *cis*-**5** solutions in three different solvents (methylcyclohexane, toluene, and acetonitrile) up to 80ºC provided no evidence of a thermally induced backward *cis*-**5** to *trans*-**3** isomerization, while the *trans*-**3** to *cis*-**5** isomerization process takes place in the three studied solvents (Scheme 20). The irreversibility of this one-way photinduced isomerization process has been attributed to the stabilization of radical **5** in solution due to the formation of the hydrogen-bonded dimeric species, as confirmed by theoretical ab-initio calculations (Paper III and X).

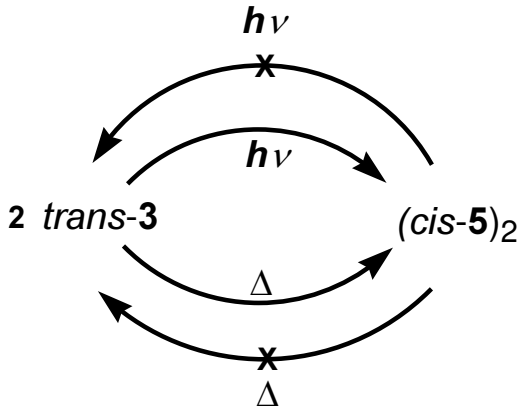

Scheme 20

This one-way thermal- and photoinduced self-assembly process represents the first example so far reported of a photomagnetic system based on a supramolecular phenomenon in which doublet species are converted into a singlet one. Along with these experiments, the

supramolecular photoinduced self-assembly process did not work with radical **4**, even though this radical also exhibits an isomerizable imino group. Indeed, independently of the polarity of the solvent used, radical **4** did not experience any *trans* to *cis* interconversion neither after irradiation at different wavelengths nor after warming up the solution. This fact has been attributed to the fact that an increase of the donor ability of the metallocene unit, i.e., permethylation of the ferrocene unit, results in an increase of the polarity of the system. This is the reason why independently of the solvent used, an external irradiation always favors an intramolecular electron transfer in front of a photoisomerization processes (Paper X).

Finally, *ab initio* calculations to help us to evaluate the structural and electronic properties of radicals **3**-**5**, and its influence on the effectiveness of photoinduced process, were carried out by Prof. J. Novoa at the University of Barcelona.[19]

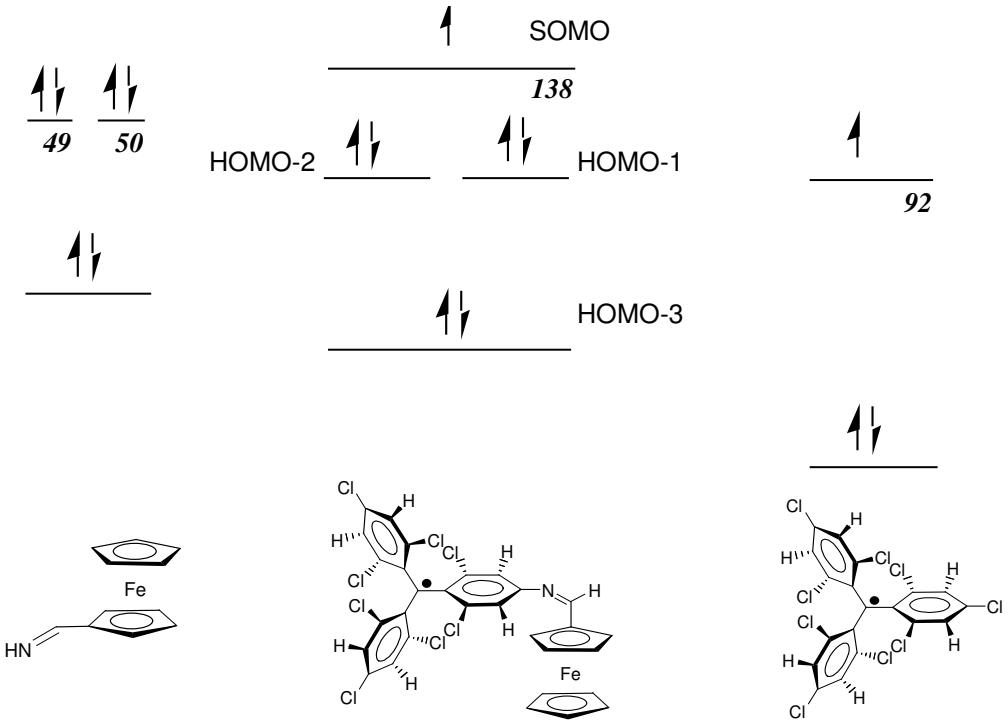

Figure 21. Energy level diagram for the frontier molecular orbitals for radical *cis*-**5** obtained from ab-initio molecular orbital calculations.

From such studies, it can be extracted that the electronic properties of these radicals are a consequence of the shape and energy distribution of the highest occupied and the lowest vacant orbitals. Figure 21 shows the energy distribution of the molecular orbitals and Figure 22 the shape of the aforementioned orbitals for radical **5**, which are nearly identical to those obtained for radical **3**. The single occupied molecular orbital (SOMO) is mostly placed on the central C of the radical unit, with a small contribution on the six-membered ring attached to the C=N group, and also on the C=N group. Below the SOMO one finds two degenerated orbitals placed on the Fe atom of the ferrocene unit. The LUMO orbital is also located on the ferrocene, with a small contribution on the C=N unit (Paper X).

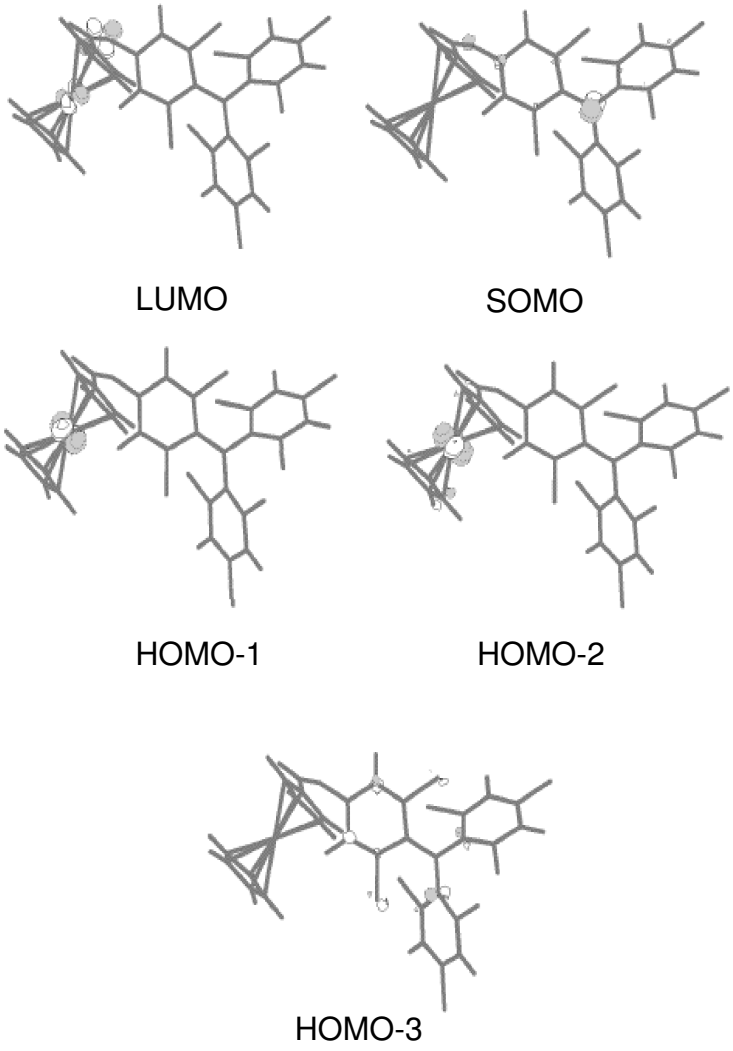

Figure 22. Ab-initio calcultation of LUMO, HOMO's and SOMO orbitals for radical *cis*-**5.**

We have also investigated the shape of the potential energy curve for the *trans-cis* isomerization to bring out more information about the thermodynamics and kinetics of the *trans-cis* isomerization. The barrier heights curves for the *trans*-**3** to *cis*-**5** and *trans*-**4** to *cis*-**6** interconversions are very similar, and present only two minima separated by a barrier, one for the *cis* and another for the *trans* isomer (see Figure 23). Surprisingly, its energy is not strongly influenced by the presence of the methyl groups in the ferrocene unit (it is only 5 kcal/mol smaller for *cis*-**5** than for the *cis*-**6**). In both radicals the *trans* form is more stable than the *cis* isomer, being the energy difference between them similar (4 and 6 kcal/mol for radicals **3-5** and **4-6**, respectively). Nevertheless, preliminary calculations on the supramolecular dimeric species evidenced a stabilization of their energies versus the corresponding *trans* form. This is probably the main reason why radical *trans*-**3** exhibits either a thermal and photinduced irreversible one-way isomerization to *cis*-**5** (Paper X),

whereas radical *trans*-**4** does not (radical *cis*-**6** is not expected to generate supramolecular species due to the presence of high steric congestions).

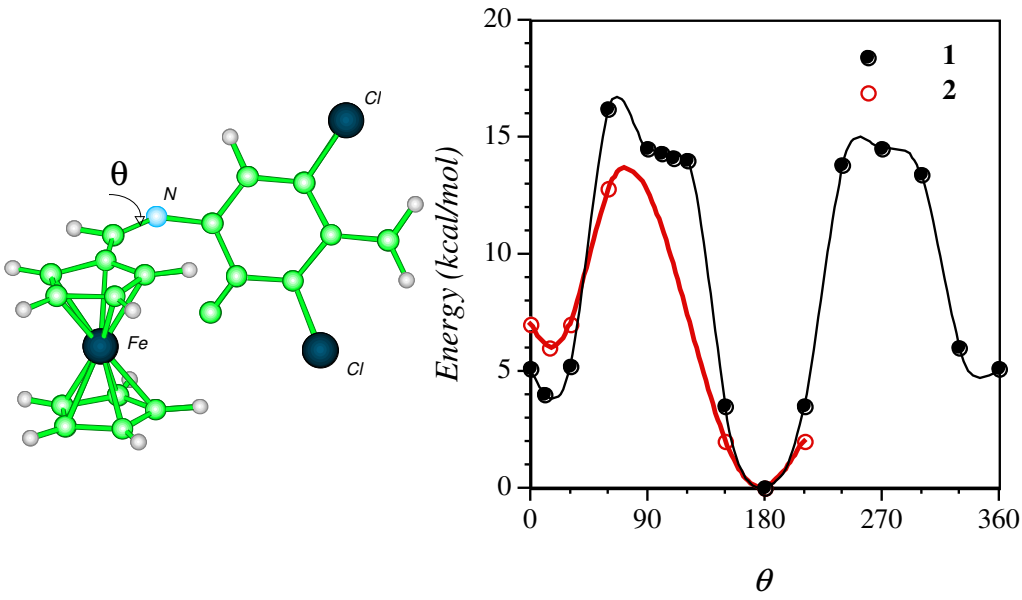

Figure 23. Ab-initio calculation of the potential energy curve for the *trans-cis* conversion for the *cis*-**3**-*trans*-**5** (black line) and *cis*-**4**-*trans*-**6** (red line) radicals,

It is also interesting the structure at θ=90°, which has the particularity that the C(ttm)-CH=N angle is colinear (180°), and, consequently, identical to that at θ=270° (see Figure 24). It proves that the thermal isomerization mechanism takes place through a linear geometry.

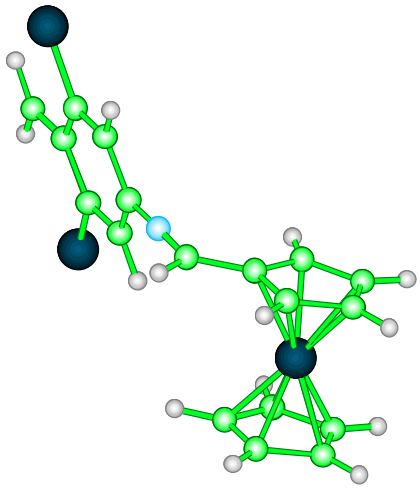

Figure 24. Minimized geometry for θ=90º obtained by ab-initio calculations

3.1.2.2 High-Spin Molecules (Intramolecular Interactions)

Metallocenes are excellent candidates to be used as magnetic couplers not only because of their rich chemistry but also because they are electroactive species whose oxidation state can be controlled by means of a chemical or electrochemical stimulus; moreover their oxidized states are of open-shell character. However, although such complexes have been successfully used as building blocks of molecular solids promoting intermolecular magnetic exchange interactions,[20] their use as intramolecular magnetic couplers is new. Prior to the present Thesis, a family of biradicals consisting of two purely organic α-nitronyl aminoxyl radicals connected by different 1,1-metallocenylene bridges had already been synthesized. In such a work, the metallocene units were shown to act as effective magnetic couplers that transmit the magnetic interactions through their skeletons, although the small spin density located on the metallocene units of these systems and the presence of intramolecular hydrogen bonds, which determines the existence of a direct intramolecular through-space magnetic interaction make these complexes not suitable candidates to study and rationalize the behaviour of 1,1-metallocenylene bridges as magnetic couplers.[21]

For this reason, the capability of metallocene units as magnetic couplers was studied along the series of polyradicals **7**-**10,** consisting of two or three polychlorinated triphenylmethyl radicals connected by a metallocenyl bridge.

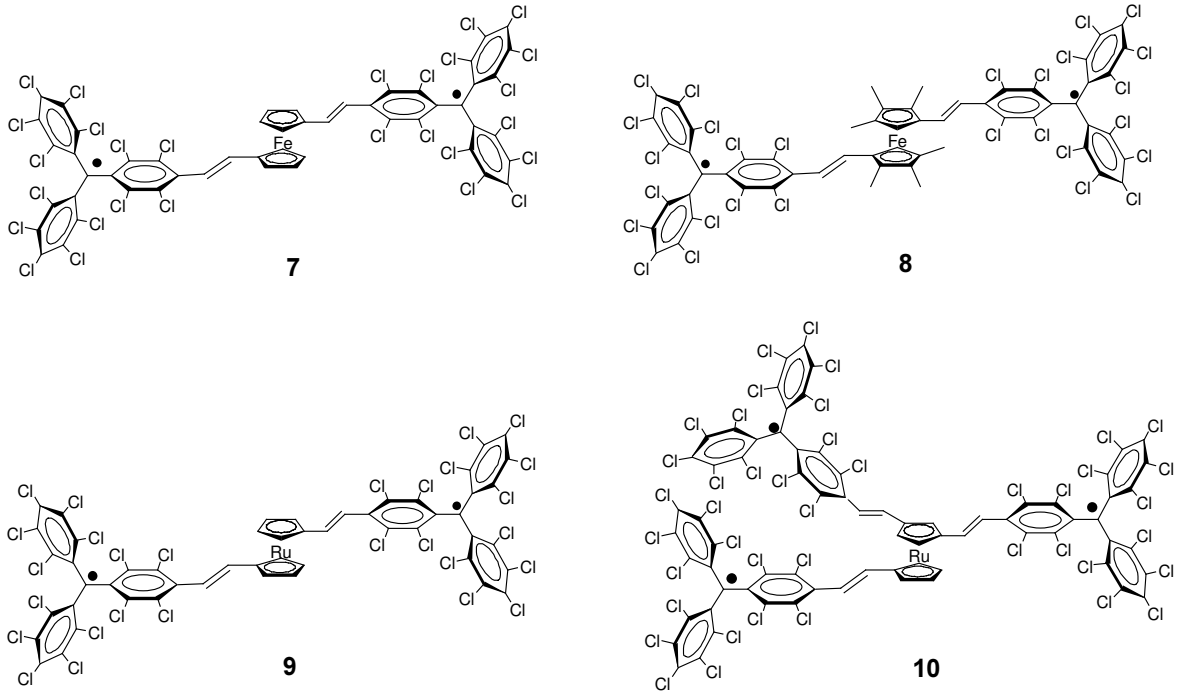

Scheme 21

The particular structure and topology of such polyradicals leads to expect non-negligible spin density on the ferrocene moiety making feasible the magnetic coupling between the two organic radical units. In addition, the location of both radical units far away from each other avoids any possibility of having intramolecular contacts, and consequently, a significant direct through-space magnetic interaction. Finally, it has to be mentioned that prior to this Thesis, the high persistence as well as the particular structural and conformational characteristics of radicals of this family, permitted not only to functionalize them but already to build pure organic open-shell dendrimers with high-spin ground states and low-spin excited states inaccessible even at room temperature, confirming the feasibility of these radicals as building blocks to construct high-spin macromolecules.

EPR solution studies: The spectrum of diradical **7** in a frozen toluene/CH_2Cl_2 (1:1) mixture shows the characteristic fine structure of a triplet species. The forbidden $\Delta m_s = \pm 2$ transition characteristic of triplet species, is also observed at the half-field region of the spectrum and the intensity of the corresponding signal (I_{pp}) was measured in the 4–100 K temperature region, indicating its magnetic ground state is the triplet state and the singlet state should be associated with a thermally accessible excited state. A separation of +10 K (7 cm^{-1}) between both states was obtained from the fitting of the $I_{pp}T$ versus T plot to the Bleaney–Bowers equation (see Figure 25) (Paper I and X). This result confirms the capability of metallocene bridges as effective magnetic couplers, although its effectiveness decreases by replacing the ferrocene unit of radical **7** by a permethylated ferrocene unit (diradical **8**) or a ruthenocene unit (diradical **9**).

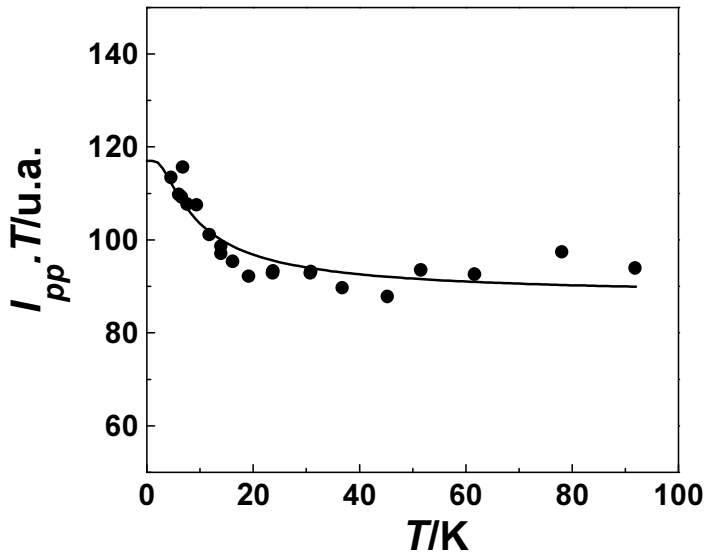

Figure 25. Temperature dependence of the $I_{pp}.T$ of diradical **7**. The closed circles represent the experimental data and the continuous lines the fit of experimental data to the Bleaney-Bowers equations

Indeed, the frozen solution spectra (below 160 K) of biradicals **8** and **9** also exhibit the typical pattern of a rigid distribution of randomly oriented triplets with axial symmetries, although in both cases the *IppT* versus *T* plot obtained from the forbidden $\Delta m_s = \pm 2$

transition indicates a paramagnetic behavior in all the temperature range studied. This results, point to the presence of almost degenerated triplet and singlet ground states.

Solid state studies: The static magnetic susceptibility, χ, of polycrystalline samples of polyradicals **7**-**9** were measured between 2 K and 300 K with a SQUID susceptometer under different external applied fields. The first observation that deserves to be commented at this point is the fact that the $\chi \cdot T$ product values at room temperature diverge from the theoretical value of 0.75 emu.K^{-1}.mol^{-1} expected for two uncorrelated S=1/2 moieties. Such outsized values have been tentatively assigned to significant orbital contributions of the remnant $[Fe^{III}Cp_2]^+$ fraction over the spin only value, as previously described for monoradical **1**-**4**. Moreover, the $\chi.T$ plots are also strongly field dependent, exhibiting larger deviations at lower fields. Although it has to be fully confirmed in future experiments, such anomalous behavior may arise from an intramolecular electron transfer process (see Scheme 22).

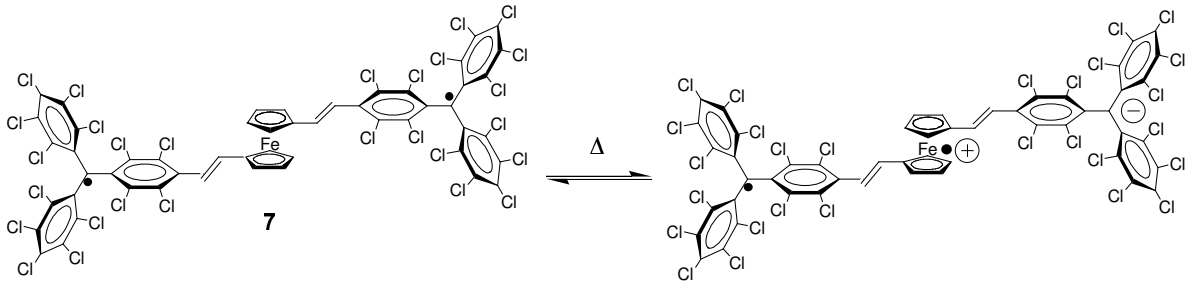

Scheme 22

A decrease of the temperature reveals a steady decrease of $\chi \cdot T$, down to 10 K, whereupon the $\chi \cdot T$ moment abruptly decreases. The magnetic susceptibility data of radicals **7**-**9** was nicely fitted to the Bleaney-Bowers equation including an additional term accounting for the presence of temperature independent paramagnetism (TIP). The resulting effective magnetic exchange coupling constant (*J/K*) are shown in Table 4. As can be observed there, the resulting *J/K* values are negative and of similar order (~ -1 K) than the Curie values so far obtained for most polychlorotriphenylmethyl monoradicals up to now described. For this reason, it can be concluded that magnetic exchange interactions may come either from intramolecular magnetic exchange interactions within the two radical units of the diradical and/or most likely from intermolecular magnetic exchange interactions between different molecules.

The main discrepancy comes from the fit of the magnetic susceptibility data of radical **7** to a Curie-Weiss law, which yields an anomalous low and negative *J/K* value, in contraposition with that obtained by EPR experiments. Due to the light nature of such magnetic exchange interactions, the presence of different conformers in solution and in solid state, may be a plausible explanation for the explanation of such divergences.

Table 4. J/K_B constant values found from the fit of experimental data to Bleaney-Bowers law for compounds **7**-**9**

Compound	J/K_B (K)	TIP (emu.mol^{-1})
7	-0.8	---[a] 0.0003[b]
8	-2.3	0.0037[a] 0.0340[b]
9	-1.1	---[a,b]

[a] Measured with an external magnetic field of 1T ;
[b] Measured with an external magnetic field of 0.1T

Finally, the static magnetic susceptibility, χ, of a polycrystalline sample of triradical **10** measured between 2 K and 300 K exhibited a quasi-paramagnetic behaviour down to low temperatures, whereupon the $\chi \cdot T$ moment abruptly decreases range studied. As previously observed for the ruthenocene diradical 9, it can be concluded that the weak (almost negligible) magnetic exchange interactions may come either from intramolecular magnetic exchange interactions and/or most likely from intermolecular magnetic exchange interactions between different molecules.

REFERENCES

1. (a) Gateschi, D; Kahn, O.; Miller, J. S.; Palacio, F. *Molecular Magnetic Materials*; Kluwer Academic: Dordrecht, **1991**. (b) Kahn, O. *Molecular Magnetism*; VCH Publishers: Weinheim, **1993**. (c) Miller, J. S.; A. J. *Angew. Chem., Int. Ed. Engl*. **1994**, *33*, 385.
2. McConnell, H. M. in *Proc. R. A. Welch Found. Chem. Res.,* Vol. *11* , **1967**, p.144.
3. McConnell, H. M. *J. Chem. Phys*., **1963**, *39*, 1910.
4. (a) Mataga, N. *Theor. Chim. Acta* **1968**, *10*, 372. (b) Borden, W. T., Ed. *Diradicals*; Wiley: New York, **1982**. (c) Iwamura, H. *Adv. Phys. Org. Chem.* **1990**, *26*, 179-253. (d) Dougherty, D. A. *Acc. Chem. Res.* **1991**, *24*, 88.
5. For selected examples of the use of *m*-phenylene as a ferromagnetic coupler, see: (a) Schlenk, W.: Braum, M. *Ber. Dtsch. Chem. Ges.* **1915**, *48*, 661. (b) Kothe, G.; Denke, K.-H.; Su¨mmermann, W. *Angew. Chem., Int. Ed. Engl.* **1970**, *9*, 906-907. (c) Calder, A.; Forrester, A. R.; James, P. G.; Luckhurst, G. R. *J. Am. Chem. Soc.* **1969**, *91*, 3724-3727. (d) Ishida, T.; Iwamura, H. *J. Am. Chem. Soc.* **1991**, *113*, 4238. Dougherty, D. A. *Mol. Cryst. Liq. Cryst.* **1989**, *176*, 25. (e) Wassermann, E.; Murray, R. W.; Yager, W. A.; Trogollo, A. M.; Smolinsky, G. *J. Am. Chem. Soc.* **1967**, *89*, 5076. (f) Tukada, H.; Mutai, K.; Iwamura, H. *J. Chem. Soc., Chem. Commun.* **1987**, 1159.
6. (a) Kasai, D. A.; Chang, W.; Dougherty, D. A. *J. Am. Chem. Soc*. **1991**, *113*, 2764. (b) Rajca, A. *J. Am. Chem. Soc.* **1990**, *112*, 5890. (b) Rajca, A.; Utamapanya, S.; Xu, J. *J. Am. Chem. Soc.* **1991**, *113*, 9235. (c) Veciana, J.; Rovira, C.; Armet, O.; Domingo, V. M.; Crespo, M. I.; Palacio, F. *J. Am. Chem. Soc.* **1991**, *113*, 2552-2561.
7. (a)Borden, W. T.; Iwamura, H.; Berson, J. A. *Acc. Chem. Res.* **1994**, *27*, 109-116. (b) Dvolaitzky, M.; Chiarelly, R.; Rassat, A. *Angew. Chem., Int. Ed. Engl.* **1992**, *31*, 180-181. (c) Kanno, F.; Inone, K.; Kago, N.; Iwamura, H. *J. Am. Chem. Soc.* **1993**, *115*, 847-850.
8. (a) Fang, S.; Lee, M.-S.; Hrovat, D. A.; Borden, W. T. *J. Am. Chem. Soc.* **1995**, *117*, 6727-6731. (b) West, A. P., Jr.; Silverman, S. K.; Dougherty, D. A. *J. Am. Chem. Soc.* **1996**, *118*, 1452-1463 and references therein.
9. (a) Armet, O., Veciana, J., Rovira, C., Riera, J., Castañer, J., Molins, E., Rius, J., Miravitlles, C., Olivella, S., Brichfeus, J. *J. Phys. Chem.***1987**, *91*, 5608. (b) Ruiz-Molina, D., Veciana, J., Palacio, F., Rovira, C. *J. Org. Chem*. **1997**, *12*, 9009.
10. Chang, H.-Ch., Miyasaka, H., Kitagawa, S. *Inorg. Chem*. **2001***, 40*, 146.
11. (a) Sato,O.; Iyoda, T.; Fujishima, A.; Hashimoto, K. *Science,* **1996,** *272*, 704. (b) Verdaguer, M. *Science,* **1996**, *272*, 698.
12. (a) Gütlich, P.; Hauser, A.; Spiering, H. *Angew. Chem. Int. Ed. Engl.* **1994**, *33*, 2024 and refs. therein. (b) Nagai, K.; Iyoda, T.; Fujishima, A.; Hashimoto, K. *Solid State Commun.* **1997**, *102*, 809.
13. Nakatsuji, S.; Mizumoto, M.; Takai, A.; Akutsu,H.; Yamada, J.; Kawamura, H.; Schmitt, S.; Hafner, K. *Mol. Cryst. Liq. Cryst.* **2000**, *348* 1.
14. (a) Hamachi, K.; Matsuda, K.; Itoh, T.; Iwamura, H. *Bull. Chem. Soc. Jpn.* **1998**, *71*, 2937. (b) Matsuda, K.; Irie, M. *Chem. Lett. 2000* 16. (c) Matsuda, K.; Irie, M.; *Tetrahedron Lett,* **2000***, 41*, 2577. (d) Matsuda, K.; Irie, M. *J. Am. Chem. Soc.* **2000**, *122*, 7195. (e) Matsuda, K.; Irie, M. *J. Am. Chem. Soc.* **2000**, *122*, 8309.
15. (a) Nakatsuji, S.; Ogawa, Y.; Takeuchi, S.; Akutsu, H.; Yamada, J.; Naito, A.; Sudo, K.; Yasuoka, N. *J. Chem. Soc., Perkin Trans.* **2000**, *2*, 1969. (b) Ojima, T.; Akutsu, H.; Yamada, J.; Nakatsuji, S.; *Chem. Lett.* **2000,** *918*. (c) Takeuchi, S.; Ogawa, Y.; Naito, A.; Sudo, K.; Yasuoka, N.; Akutsu, H.; Yamada, J.; Nakatsuji, S. *Mol. Cryst. Liq. Cryst*. **2000**, *345*, 167.
16. (a) K. Hamachi, K. Matsuda, T. Itoh, H. Iwamura, *Bull. Chem. Soc. Jpn*. **1998**, *71*, 2937. (b) K. Matsuda, M. Irie, *Chem. Lett*. **2000**, 16. (c) K. Matsuda, M. Irie, *Tetrahedron Lett.* **2000**, *41*, 2577. (d) K. Matsuda, M. Irie, *J. Am. Chem. Soc*. **2000**, *122*, 7195. (e) K. Matsuda, M. Irie, *J. Am. Chem. Soc.* **2000**, *122*, 8309. (f) Ojima, T.; Akutsu, H.; Yamada, J.; Nakatsuji, S., *Polyhedron***, 2001**, *20*, 1335. (g) Karasawa, S.; Koga, N., Polyhedron, **2001**,*20*, 1387.
17. Sander, W.; Bucher, G.; Reichel, F.; Cremer, D. *J. Am. Chem. Soc.* **1991**, *113*, 5311.
18. Bush, L. C.; Heath, R. B.; Berson, J. A.; *J. Am. Chem. Soc*. **1993**, *115*, 9830.

19.We have carried out UB3LYP calculations on the doublet ground state of the four isomers using the LANL2DZ basis set (which uses the Wadt-Hay effective core potentials for the core electrons, while a basis set of double zeta quality is used for the outer electrons). The doublet state is for these radicals the ground state and presents at the UB3LYP/LANL2DZ level a very small spin contamination. The calculations were done on the crystal geometry of the *trans*-1 isomer, while the optimum UB3LYP/LANL2DZ geometry of the doublet was used for all other isomers, as no crystal structure were available for them.
20.Miller, J. S. and Epstein, A. J. *Angew. Chem., Int. Ed. Engl.*, **1994**, *33*, 385 and references therein.
21.Jürgens, O.; Vidal-Gancedo, J.; Rovira, C.; Wurst, K.; Sporer, C.; Bildstein, B.; Schottenberger, H.; Jaitner, P. and Veciana, J. *Inorg. Chem*. **1998**, *37*, 4547.